Journal of Medicinal Chemistry

Article

Small Molecule Proprotein Convertase Subtilisin/Kexin type 9 (PCSK9) Inhibitors: Hit to Lead Optimization of Systemic Agents

Allyn Timothy Londregan, Liuqing Wei, Jun Xiao, Nathanael G Lintner, Donna N. Petersen, Robert Dullea, Kim F. Mcclure, Michael W Bolt, Joseph S Warmus, Steven B. Coffey, Chris Limberakis, Julien Genovino, Benjamin A. Thuma, Kevin D. Hesp, Gary E Aspnes, Benjamin Reidich, Christopher T. Salatto, Jeffrey R Chabot, Jamie H.D. Cate, Spiros Liras, and David W. Piotrowski

J. Med. Chem., **Just Accepted Manuscript** • DOI: 10.1021/acs.jmedchem.8b00650 • Publication Date (Web): 07 Jun 2018

Just Accepted

ACS Publications

is published by the American Chemical Society. 1155 Sixteenth Street N.W., Washington, DC 20036

Small Molecule Proprotein Convertase Subtilisin/Kexin type 9 (PCSK9) Inhibitors: Hit to Lead Optimization of Systemic Agents

Allyn T. Londregan,[*,†] *Liuqing Wei,*[†] *Jun Xiao,*[†] *Nathanael G. Lintner,*[‡] *Donna Petersen,*[#] *Robert G. Dullea,*[§] *Kim F. McClure,*[∥] *Michael W. Bolt,*[ǂ] *Joseph S. Warmus,*[†] *Steven B. Coffey,*[†] *Chris Limberakis,*[†] *Julien Genovino,*[†] *Benjamin A. Thuma,*[†] *Kevin D. Hesp,*[†] *Gary E. Aspnes,*[∥] *Benjamin Reidich,*[§] *Christopher T. Salatto,*[§] *Jeffrey R. Chabot,*[^] *Jamie H. D. Cate,*[‡,⊥,◊,=] *Spiros Liras*[∥] *and David W. Piotrowski*[*,†]

[†]Pfizer Medicinal Chemistry, Groton, Connecticut 06340, United States

[‡]Department of Molecular and Cell Biology, University of California, Berkeley, Berkeley, California, 94720, United States

[∥]Pfizer Medicinal Chemistry, Internal Medicine Research Unit, Pfizer Worldwide Research and Development, Cambridge, Massachusetts, 02139, United States

[#]Primary Pharmacology Group, Pharmacokinetics, Dynamics and Metabolism, Pfizer Worldwide Research and Development, Groton, Connecticut, 06340, United States

[ǂ]Drug Safety Research & Development, Pfizer Worldwide Research & Development, Cambridge, Massachusetts, 02139, United States

[^]Pfizer Pharmacokinetics, Dynamics and Metabolism Modeling and Simulation, Pfizer Worldwide Research and Development, Cambridge, Massachusetts, 02139, United States

[§]Internal Medicine Research Unit, Pfizer Worldwide Research and Development, Cambridge, Massachusetts, 02139, United States,

[⊥]QB3 Institute, University of California, Berkeley, Berkeley, California, 94720, United States

[=]Department of Chemistry, University of California, Berkeley, Berkeley, California, 94720, United States

[◊]Physical Biosciences Division, Lawrence Berkeley National Laboratory, Berkeley, California, 94720, United States

KEYWORDS: PCSK9, proprotein, convertase, lipoprotein, LDLR, protein synthesis, translation, LDL-C

ABSTRACT: The optimization of a new class of small molecule PCSK9 mRNA translation inhibitors is described. The potency, physicochemical properties and the off-target pharmacology associated with the hit compound (**1**) were improved by changes to two regions of the molecule. The last step in the synthesis of the congested amide center was enabled by three different routes. Subtle structural changes yielded significant changes in pharmacology and off-target margins. These efforts led to the identification of **7l** and **7n** with overall profiles suitable for in vivo evaluation. In a 14-day toxicology study, **7l** demonstrated an improved safety profile vs. lead **7f**. We hypothesize that the improved safety profile is related to diminished binding of **7l** to non-translating ribosomes and an apparent improvement in transcript selectivity due to the lower strength of **7l** stalling of off-target proteins.

INTRODUCTION

Proprotein Convertase Subtilisin/Kexin type 9 (PCSK9) is a secreted 71 kDa serine proteinase consisting of an N-terminal prodomain, a catalytic domain, and a C-terminal domain. The protein is primarily expressed in the liver and is exported to plasma where it down regulates cell surface levels of the low density lipoprotein receptor (LDLR) via endocytosis and lysosomal degradation.[1] The affinity of PCSK9 for LDLR becomes progressively tighter at lower pH with the equilibrium dissociation K_d reaching low nanomolar concentrations at lysosomal pH.[2] After initial endocytosis, the PCSK9-LDLR complex is believed to undergo a sorting process within the endosome. By a mechanism potentially involving accessory proteins, LDLR is either recycled[3] to the cell surface or carried to its destruction in the lysosome with PCSK9.[4] As such PCSK9 has a significant role in the maintenance of plasma low density lipoprotein cholesterol (LDL-C), a primary risk factor for cardiovascular disease. Human genetics and the PCSK9 neutralizing antibodies confirm the important role of PCSK9 in LDL-C regulation. Individuals with PCSK9 loss of function mutations have both lower LDL-C and reduced cardiovascular risk.[5] Equally, the PCSK9 antibodies alirocumab, evolocumab and bococizumab have demonstrated 35-69% reduction in plasma after 12 weeks of biweekly parenteral administration.[6]

Although antibodies targeting mature PCSK9 are the most advanced clinically, other points of intervention and modalities have been reported. In all cases, small molecule progress has lagged behind. Unlike the majority of the proprotein convertase family members, the prodomain of PCSK9 remains tightly bound to the catalytic domain in its mature form.[7] This is attributed to the lack of a secondary cleavage event within the prodomain thought to destabilize its association with catalytic subunit of the convertase. In spite of this, attempts have been made to target the hydrolase center (Ser386, His226, Asp186) of mature PCSK9 based on computed models

wherein the prodomain has been removed.[8] The fact that dissociation of the prodomain can be observed in the context of domain exchange experiments supports potential access to the catalytic triad.[9] In principle, an active site binder could displace the prodomain from the catalytic domain leading to improper folding and secretion of PCSK9. Nevertheless, the demonstration that the proteolytic activity is not required for PCSK9 functional regulation of LDLR[10] puts into question the effectiveness of molecules designed to bind the catalytic triad or neighboring pockets of secreted PCSK9.[2a] The functional action of PCSK9 is therefore believed to be more a result of pH sensitive protein-protein interactions over diverse regions of its surface.[11] To obtain competitive inhibitors would then require inhibition of PCSK9's interaction with the LDLR. PCSK9 is the preferred target between the two proteins as acting directly at the LDLR presents the risk of interfering with its role in LDL-C regulation. One of the primary contact patches with PCSK9 at neutral pH is the epidermal growth factor precursor homology domain A (EGF-A) of the LDLR. While parenteral anti-PCSK9 antibodies and adnexins are capable of gaining affinity by extending beyond this small (530 Å) and relatively featureless EGF-A interacting region on PCSK9, peptide approaches have struggled to achieve the size and properties sufficient to facilitate oral administration.[12] For small molecules, gaining sufficient perch on the flat EGF-A interacting region of PCSK9 is understandably even more challenging but a recent disclosure suggests that the adjacent P'-helix site offers some hope for disruption of the PCSK9/LDLR interaction with small molecules.[13] A review of other small molecule inhibitors has been disclosed.[14]

For these reasons attempts have been made to target PCSK9 prior to its maturation. The recent demonstration that the PCSK9 catalytic domain is capable of intermolecular (in trans) substrate cleavage has led to the hope of identifying small molecules that can inhibit the intramolecular (in

cis) auto-processing of proPCSK9.[15] The inhibition of PCSK9 mRNA translation has also been explored. Both antisense locked nucleic acids and short interfering RNA (siRNA) of PCSK9 messenger RNA have progressed to human clinical trials with significant PCSK9 and LDL-C lowering being reported for the siRNA.[16]

Previously, we described the identification of small molecule inhibitors of PCSK9 mRNA translation by a cell-based HTS designed to find molecules that decreased PCSK9 secretion to the cell media.[17] From this effort, PF-00932239 (**1**) was identified as a hit (Table 1) and subsequently shown to decrease PCSK9 secretion and increase cell surface LDLR and LDL-C uptake in recombinant and native cell lines via a mechanism attributed to the inhibition of PCSK9 early in its translation. PF-06446846 (**7f**) was later identified as an advanced prototype suitable for biological, safety and mechanistic evaluation, the details of which were recently described.[18] In parallel, efforts to achieve a liver-selective PCSK9 inhibitor via a pro-drug strategy were also explored.[19] Herein, we disclose our medicinal chemistry efforts to transform **1** into molecules with high systemic bioavailability and an improved balance of safety and efficacy suitable for further exploration.

RESULTS AND DISCUSSION

As discussed above, compound **1** was identified from a cell-based HTS. Subsequent localization of the inhibition point in protein translation informed the development of a high capacity luciferase reporter assay (PCSK9 ProLuc) to monitor the translation of a truncated human PCSK9 (1-152) construct within transfected Huh7 cells as a surrogate for the native protein. This was the primary assay initially used to screen for compounds with improved pharmacology. The molecular weight and LogD of **1** were acceptable, as were permeability (RRCK) and safety (dofetilide binding, CYP inhibition, cell toxicity) assessments (see Table 1).

However, the intrinsic clearance of **1** in rat liver microsomes (RLM) was high, when compared to human, and represented an initial hurdle in the development of a viable rodent tool compound. The initial optimization process was therefore designed to improve potency and reduce clearance of compounds through the careful modulation of lipophilicity, while maintaining the favorable properties of **1**. A screening cascade was implemented to facilitate identification of an orally bioavailable tool compound suitable for in vivo studies. Parallel assessments of activity (PCSK9 ProLuc), rat and human liver microsomal (HLM) stability, and in vitro safety were used to triage compounds.

Table 1. Pharmacological, Absorption, Metabolism, and Safety Properties of 1

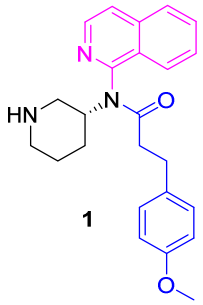

1

MW: 389.1, LogD[a]: 1.1, LipE[b]: 4.5	
PCSK9 ProLuc IC_{50} (μM)	2.63
Cell Toxicity (μM)[c]	> 20
RRCK (Papp, 10^{-6} cm/sec)[d]	5.4
RLM Clint (μL/min/mg)	> 510
HLM Clint (μL/min/mg)	20.6
CYP (% inh at 3 μM)	1A2, 2D6, 2C9, 3A4 < 20 %
DOF K_i (μM)[e]	13

[a]LogD determined by shake flask method. [b]LipE = -LogIC_{50}PCSK9 ProLuc – LogD. [c]CellTiter-Glo® ATP viability assay. [d]RRCK = Modified Madin-Darby permeability assay.[20] [e]DOF = dofetilide fluorescence polarization binding assay.

Although the chemical series represented by **1** appeared highly amenable to rapid analogue generation, synthetic modifications were initially found to be quite challenging. The common obstacle to all analogues was the formation of the central tertiary amide bond. Compound **1** was divided into three fragments: the heterocyclic head group (magenta), the acyl linker (blue), and the amine (black), for the purpose of exploring the SAR. Mindful of the desire to rapidly explore the chemical space around this chemotype, we developed three complementary synthetic methods to expand the SAR via singleton and parallel synthetic methods (see Scheme 1). In Route A, an Abramovitch rearrangement[21] of amide **4** and *N*-oxide **5** was performed to afford **6**, which was subsequently deprotected under acidic conditions to give **7**. This route was useful for initial SAR generation where the amine and amide fragments could be readily explored by parallel chemistry starting from isoquinoline *N*-oxide and diverse sets of mono-Boc diamines and carboxylic acids. No compounds more potent than **1** were found (data not shown) so further analogue work was restricted to use of amine **2**. It was soon determined that isoquinoline-*N*-oxide was a uniquely competent reaction partner in the Abramovitch rearrangement, and that diversification to mono-heterocyclic *N*-oxides was complicated by low conversions and regiochemical mixtures of products. As such, a three-step sequence (Route B) was developed that would allow for more significant variation. Palladium-mediated coupling of **2** with 2-bromopyridine **8** afforded amine **9b**, which was then coupled with various carboxylic acids to give analogues **7**, after Boc-deprotection. This sequence, however, was less tolerant to diverse substrates than anticipated. The initial Buchwald-Hartwig amination required significant

optimization and was found to be highly substrate-specific. Furthermore, amines **9a**, **9b** were found to be a poor amidation partners, presumably due to steric hindrance and their electron-deficient nature. Ultimately, Route B proved to be most useful for gram scale preparation, where varied substrates were not utilized. Route C was the most successful diversity-oriented approach for analogue generation. In this sequence, Boc-protected amine **2** underwent an S_NAr reaction with 2-halo-azine-*N*-oxide **10** to give **11**, which was directly coupled with **3** to yield **12**. The *N*-oxide and Boc-protecting group were then readily removed under mild conditions[22] to afford the desired analogues **7**. In this case, the S_NAr reaction is electronically enhanced by the *N*-oxide, which further enables the amide coupling of **11** and **3** via an intra-molecular activation mechanism.[23]

Scheme 1. Synthetic Approaches to Tertiary Benzamides[a]

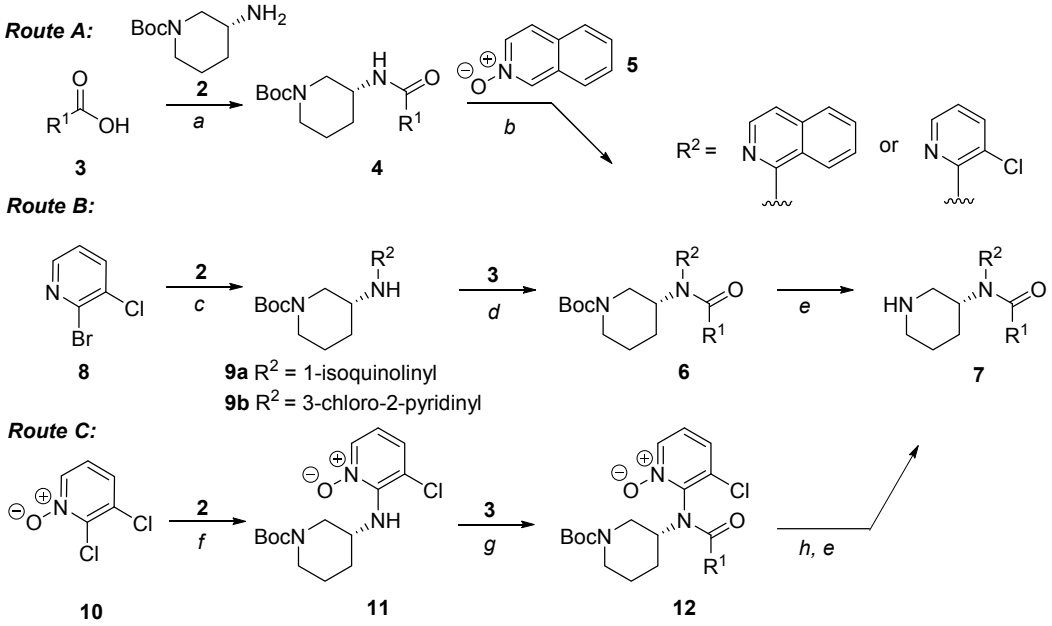

[a]Reagents and conditions: (a) 1,1'-carbonyldiimidazole, DMF, 30 °C. (b) trifluoromethanesulfonic anhydride, 2,6-lutidine, DCM, -30 to 25 °C. (c) chloro(di-2-norbornylphosphino)(2-dimethylaminoferrocen-1-yl) palladium (II), KO*t*Bu or NaO*t*Am, toluene, 105-110 °C. (d) **3**, oxalyl chloride, DCM, 0-25 °C, then LHMDS, THF, 25 °C or

iPr_2EtN, DMAP, THF, 65 °C. (e) HCl in 1,4-dioxane or TFA in DCM, 25 °C. (f) *i*Pr_2EtN, DMAP, CsF, *n*BuOH, 100 °C. (g) bromotripyrrolidinophosphonium hexafluorophosphate (PyBroP), *i*Pr_2EtN, THF. (h) Et_3SiH, MeOH, 10% Pd-Al_2O_3.

Using a parallel-enabled version of the chemistry developed for route A, the amide vector of **1** was optimized using a diverse set of readily available carboxylic acids. Of note was the discovery of the weakly active biphenyl analogue **7a** (Table 2). Most significantly, this modification conferred improved intrinsic clearance, but at the expense of potency. A concise library protocol (Scheme 2) was therefore developed to quickly assess the SAR of more diverse para-heterocyclic benzoyl amides, with the goal to mitigate this deficiency. A straightforward Suzuki coupling of heterocyclic halides with boronate ester **14a** followed by Boc-deprotection, afforded several new analogues. Compounds **7b**, **7c** and **7d** had significantly improved profiles, with the latter being the first analogue with both sub-micromolar activity (PCSK9 Pro-Luc assay) and favorable ADME properties. Further potency improvements were achieved with *N*-triazolopyridine variant **7e**, which was synthesized from the appropriate benzoic acid **20** obtained via the sequence found in Scheme 3.

Scheme 2: Library-Expansion of the Benzamide Vector[a]

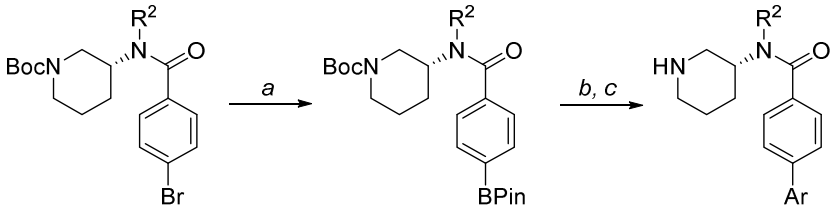

[a]Reagents and conditions: (a) Bis(pinacolato)diboron, KOAc, $PdCl_2$(dppf), 1,4-dioxane, 85 °C. (b) ArX, Cs_2CO_3, $PdCl_2$(dppf), 1,4-dioxane, 85 °C. (c) HCl, 1,4-dioxane, 25 °C.

Scheme 3. Synthesis of varied *N*-triazolo-biaryl acids[a]

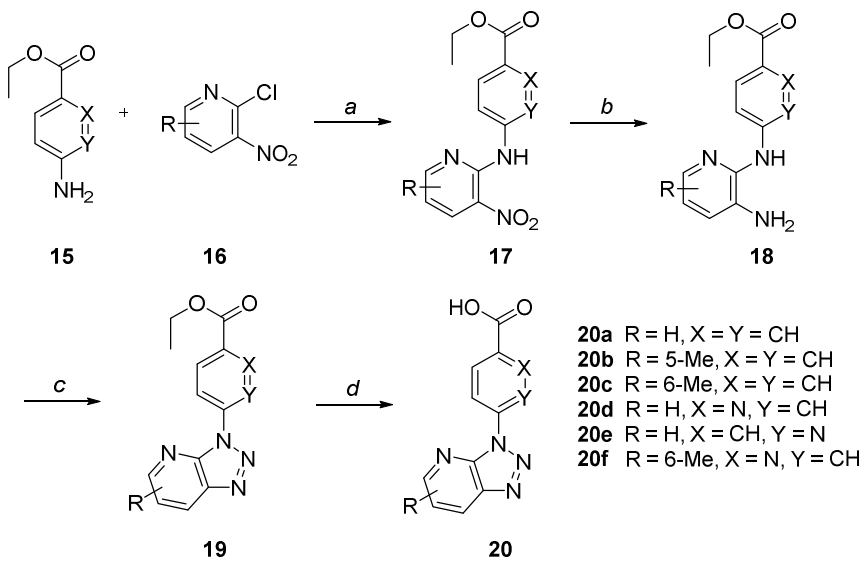

[a]Reagents and conditions: (a) $Pd(OAc)_2$, K_2CO_3, (±)-2,2′-bis(diphenylphosphino)-1,1′-binaphthalene, NaI, toluene, 110 °C. (b) Raney-Ni, H_2, EtOH, 25 °C. (c) $NaNO_2$, AcOH, H_2O, 0-25 °C, (d) NaOH, MeOH, 60 °C.

Initial attempts to further improve the potency and ADME properties of the compounds through modification of the isoquinoline moiety were not fruitful. Briefly, insertion of nitrogen atoms into the bicyclic ring (i.e. isomeric naphthyridines) or mono-substitution of the 5, 6, 7 or 8-position with small substituents (e.g. F, Me, OMe) provided no potency or ADME advantage (data not shown). Thus, our attention was directed towards an isosteric replacement for the isoquinoline moiety. As shown in Table 2, 3-chloropyridine served this purpose well. The direct comparator **7f** to isoquinoline **7e** was equipotent, sufficiently stable in liver microsomes, and exhibited modestly improved LipE (**7f** = 6.0 vs **7e** = 5.4) suggesting that future analogues would benefit from this modification. Distomer **7g** was also prepared, but it was significantly less potent. The greater potency for *R*-enantiomers is consistent with previous findings associated with **1**. Therefore, all subsequent analogues used (*R*)-3-aminopiperidine **2** as their starting points.

As previously reported,[18] compound **7f** was advanced into in vivo safety and efficacy studies, which are briefly summarized here. During the 14 d dosing period, **7f** was tolerated when orally administered at doses of 5, 15, and 50 mg/kg daily to male Sprague Dawley rats. A reduction in total cholesterol (30%) and LDL (58%) was observed at 50 mg/kg/day. However, decreased cellularity of the bone marrow also occurred at this dose that was associated with decreases in hematocrit and hemoglobin (~9-10%), decreased total nucleated cell counts (30%), absolute maturing (48%), proliferating (32.9%), and total (46%) erythroid cells, decreased white blood cells (52%), lymphoyctes (54%), monocytes (63%), eosinophils (54%) and basophils (100%), as well as decreased total T cells (54%), helper T cells (54%), cytotoxic T cells (54.5%), and B cells (58%). In addition, minimal single cell necrosis of the crypt cells in the ileum was observed at 50 mg/kg/day. No dose-limiting changes were noted at the 5 and 15 mg/kg dose level when compared to vehicle.

In consideration of these toxicology findings, which were not evident in the upfront CellTiter-Glo® ATP viability assay, in vitro bone marrow cellular toxicity assays for rat (initial toxicology species, rat lineage (-) cells) and human ($CD34^+$ cells)[19] were developed to screen for future compounds devoid of bone marrow effects. Indeed, when **7f** was assessed in the rat lineage (-) assay, it reduced cell viability (IC_{50} = 1.2 μM) within three-fold margin of its functional activity (PCSK9 Pro-Luc IC_{50} = 0.38 μM). As such, all new compounds would be assessed for rat bone marrow toxicity alongside assays in the existing screening funnel.

Without a clear understanding of the SAR driving bone marrow toxicity, we initiated point mutations based on structure **7f**. A methyl group position scan of the triazolopyridine of **7f** resulted in the equipotent 5-methyl **7h** and 6-methyl **7i** analogues. Other isomeric methylated variants (data not shown) were significantly less potent. Of note, **7i** showed a significant

improvement in bone marrow toxicity (rat lineage (-) IC_{50} > 19.7 μM) while **7h** only had a two-fold margin. This suggested that seemingly minor modifications to our lead series could be fruitful in yielding improved molecules. The benzoyl moiety was also modified to give picolinamide **7j** and nicotinamide **7k** analogues. Diazine variants of this ring led to compounds with intrinsic microsomal clearances that were essentially reduced to the limit of assay detection, presumably due to lowered LogD, but these changes generally resulted in lower potencies (data not shown). The combination of picolinamide and the beneficial 6-methyl group addition led to **7l**, which gratifyingly maintained favorable ADME and potency while exhibiting a >30-fold window between bone marrow toxicity and PCSK9 Pro-Luc activity. Analogues containing heterocycles other than triazolopyridine with sufficient potency and ADME properties were also re-examined using a similar single point mutation strategy (Table 2).

Table 2. Potency and Properties of Selected Analogues

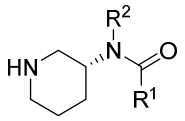

7a-o

Compound	R^1	R^2	PCSK9 ProLuc IC_{50} (μM)[a]	PCSK9 ELISA IC_{50} (μM)[a]	LogD[b]	LipE[c]	HLM Cl_{int}[d]	RLM Cl_{int}[d]	DOF K_i (μM)[e]	Cell Toxicity IC_{50} (μM)
7a	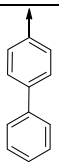	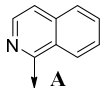 **A**	54%[h]	39%[h]	2.5	2.4	10.7	57.7	2.2	-
7b	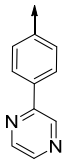	**A**	4.30	9.32	0.7	4.7	11.0	123	>40.0	>20[f]
7c	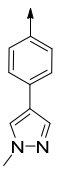	**A**	1.06	2.38	0.9	5.1	13.3	-	16.0	2.9[f]

7d	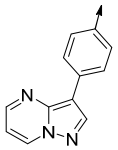	**A**	0.69	1.29	1.1	5.4	14.5	31.2	5.4	1.4[f]
7e	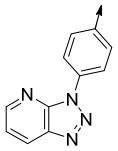	**A**	0.39	0.90	1.4	5.4	21.8	-	15.8	-
7f	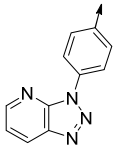	 **B**	0.38	0.82	0.8	6.0	9.7	18.2	18.1	1.2[f]
7g (S)			61%[h]	24%[h]						>20[f]
7h	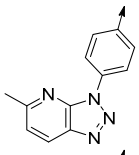	**B**	0.45	0.90	1.2	5.5	9.0	38.5	34.0	1.0[f]
7i	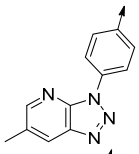	**B**	0.41	0.78	1.2	5.6	8.8	16.5	3.3	>19.7[f]
7j	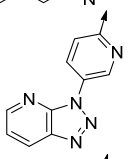	**B**	0.71	1.44	0.3	6.0	<8.0	15.3	28.8	>12.7[f]
7k	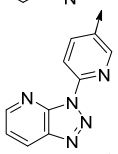	**B**	4.10	9.24	0.1	5.6	<8.0	14.7	12.7	-
7l	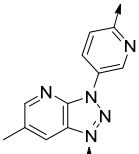	**B**	0.85	1.37	0.7	5.7	9.3	15.1	5.9	>20[f]/27.1[g]
7m	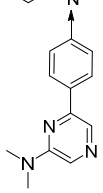	**B**	-	2.97	1.37	-	18.2	-	14.1	30.1[g]
7n	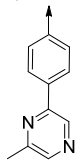	**B**	-	2.82	1.37	-	<8.0	-	38.2	43.7[g]

7o	**B**	-	3.08	1.07	8.7	-	38.4	19.6[g]

[a]Values are reported as geometric means (n > 3). Please see supporting information for the number of experiments and associated error. [b]LogD determined by shake flask method. [c]LipE = -LogIC$_{50}$PCSK9 ProLuc–LogD. [d]Intrinsic clearance μL/min/mg. [e]DOF = dofetilide fluorescence polarization binding assay. [f]CellTiter-Glo® rat bone marrow cell toxicity with puromycin as high point effect (HPE) standard. [g]CellTiter-Glo® rat bone marrow cell toxicity with **7f** as the HPE standard. [h]Percent effect at 20 μM.

In order to establish an in vitro/in vivo toxicological correlation to help differentiate the analogues of interest, a group of compounds were selected for a side-by-side safety assessment in rats at a 50 mg/kg dose. The 50 mg/kg dose is meaningful because this dose of **7f** elicited the in vivo effects on rapidly proliferating cells. Thus, **7f**, **7g**, **7i**, **7j**, and **7l** were selected as they represent analogues that span the ranges of potencies in both the PCSK9 Pro-Luc and rat lineage (-) assays (Figure 1).

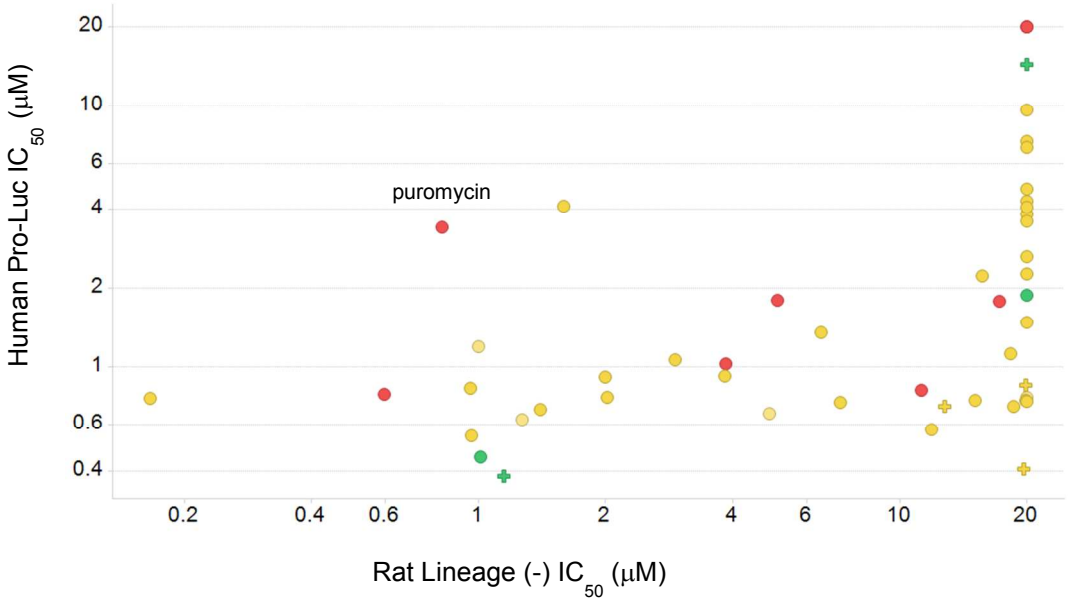

Figure 1: Rat Lineage (-) IC_{50} vs. Human Pro-Luc IC_{50}. Summary of in vitro toxicity/potency correlations. Markers are colored by RRCK (AB flux, P_{app}, 10^{-6} cm/sec) permeability, where red < 2, yellow 2-10, and green > 10. Plus-shaped markers indicate compounds also assessed in vivo.

A 14-day oral gavage toxicology study in male rats (5/group) administered vehicle or one of five different compounds at a dose of 50 mg/kg was conducted. Mortality, clinical signs and hematological endpoints were monitored throughout the course of the study. Toxicokinetic analysis was performed at 1, 3, 6, and 24 h post-dose on day 14. Importantly, after necropsy on day 15, key microscopic evaluations of bone marrow, ileum, duodenum, jejunum, and liver were conducted. Based on AUC (ng•h/mL), the exposure was within four-fold for all compounds dosed. Although decreased bone marrow cellularity and crypt cell necrosis previously observed in rats administered **7f** were also observed in this study, no other compounds tested in this study had these findings. A discolored/mottled liver was observed with all compounds tested. Hepatocyte vacuolation was observed in animals given **7i**, which was not considered dose limiting. These results confirmed that compounds with rat lineage (-) assay IC_{50} values greater than **7f** had no evidence of bone marrow or crypt cell toxicity. The results are depicted graphically in Figure 2.

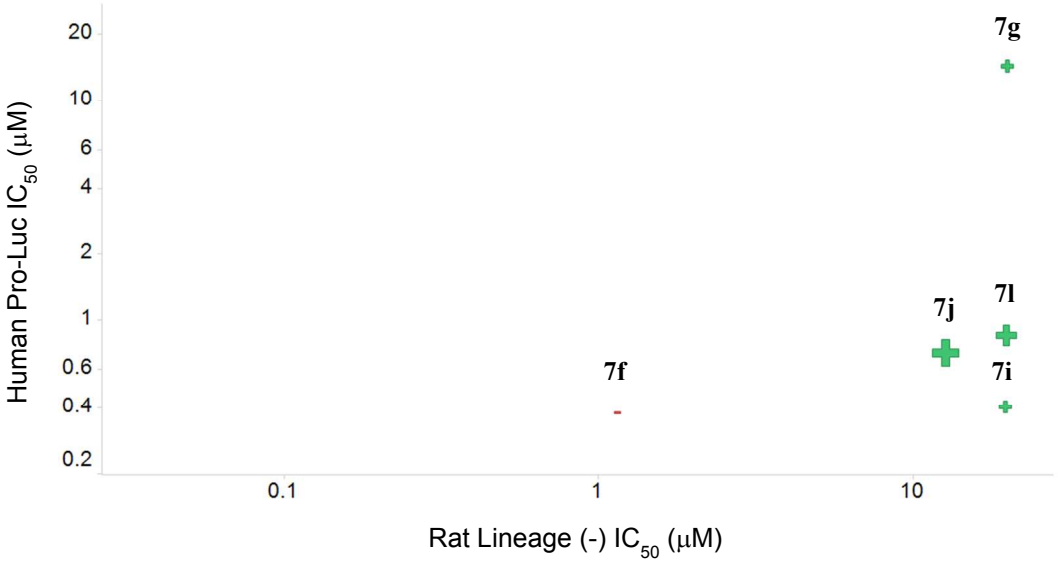

Figure 2: Rat Lineage (-) IC_{50} vs. Human Pro-Luc IC_{50}. Summary of in vitro toxicity/potency correlations. Markers are colored by white blood cell toxicity where red is white blood cell toxic and green is not white blood cell toxic. Shapes are sized by area under the curve (AUC) for the total drug exposure vs. time.

After having established an in vitro/in vivo toxicology correlation, changes to the screening funnel were instituted to further refine compound selection for additional in vivo work. Two changes were made aimed at defining more stringent selection criteria: (1) use of an enzyme-linked immunosorbent assay (ELISA) (PCSK9 ELISA) to assess potency and (2) use of compound **7f** as the high point effect (HPE) standard in the rat lineage (-) assay. It was anticipated that the former change would provide a more realistic assessment of PCSK9 inhibition since it employed the native, human full-length PCSK9 construct. In general, the two primary pharmacology assays correlated well, especially for the more potent compounds. For example, compare **1** (PSCK9 ProLuc IC_{50} = 2.63 μM vs. PCSK9 ELISA IC_{50} = 8.37 μM) and **7f** PSCK9 ProLuc IC_{50} = 0.38 μM vs. PCSK9 ELISA IC_{50} = 0.82 μM). The latter change was

instituted to reflect the correlation between in vitro and in vivo toxicity for **7f**. For example, compare **7l**, rat lineage (-) IC_{50} (puromycin HPE) > 20 μM vs. rat lineage (-) IC_{50} (**7f** HPE) = 27.1 μM.

On the basis of these newly delineated criteria, **7l** emerged as a compound with the best balance of potency in the PCSK9 ELISA assay, minimal toxicity in the rat lineage (-) assay and tolerability in vivo. However, it still had an undesirable ion channel profile as judged from low micromolar activity in the dofetilide binding assay. This was confirmed with hERG patch clamp data (hERG IC_{50} = 3.56 μM). Therefore, we evaluated a wider range of compounds that could lead to compounds that maintained the desirable qualities, have an increased window versus bone marrow toxicity and an improved hERG profile. On the basis of the favorable dofetilide profile of **7b**, pendent pyrazines were further explored that resulted in identification of compounds **7m** and **7n**. Both of these compounds showed lower bone marrow toxicity and were less potent in the hERG patch clamp assay (**7m**, hERG IC_{50} = 43.2 μM; **7n**, hERG IC_{50} = 59.8 μM). In anticipation of in vivo safety studies, rat and non-human primate PK studies were performed. Of note, the presence of an active metabolite **7o** was detected following administration of **7m** to rats. Despite negligible levels of **7o** detected in non-human primate (in vitro and in vivo) and human (in vitro), the increased potency in the rat lineage (-) cell assay and the demonstrated correlation of this assay to rat in vivo toxicity precluded **7m** from further consideration.

On the basis of the promising profiles of **7l** and **7n**, extensive ADME and safety analyses were performed in anticipation of advancing an in vivo tool. The data in comparison to former lead compound **7f** is shown in Table 3.

Table 3. Pharmacological, ADME and in vitro Safety Properties of 7f, 7l and 7n

	7f	**7l**	**7n**
MW	433.9	448.9	407.9
clogP	2.1	1.5	2.0
LogD[a]	0.8	0.7	0.8
Cell Toxicity (μM)[b]	> 20	> 20	-
RRCK (Papp, 10^{-6} cm/sec)[c]	15.0	6.2	10.5
MDR1-MDCK AB (10^{-6} cm/sec)	1.5	1.3	0.7
MDR1-MDCK BA (10^{-6} cm/sec)	20.6	19.9	20.0
CYP IC_{50} (μM) or % inhbition at 3 μM	1A2, 2D6, 2C9, 3A4 > 30 μM	1A2, 2D6, 2C9, 3A4 all < 13%	1A2, 2D6, 2C9, 3A4 > 30 μM
Fraction unbound (rat plasma)	20%	24%	41%
hERG IC_{50} (μM)[d]	8.5	3.6	59.8
Cerep panel of 72 assays screened at 10 μM	3 targets with K_i/IC_{50} < 10 μM	2 targets with K_i/IC_{50} < 10 μM	1 target with K_i/IC_{50} < 10 μM

[a]LogD determined by shake flask method. [b]CellTiter-Glo® ATP viability assay. [c]RRCK = Modified Madin-Darby permeability assay. [d]hERG = human Ether-a-go-go-Related Gene patch-clamp assay.

Compounds **7l** and **7n** were assessed in advanced in vivo safety studies. Of note, **7l** was assessed in a 14-day rat toxicology study at doses of 50, 150 and 500 mg/kg/day. Although mortality and dose-limiting toxicity was observed at ≥ 150 mg/kg/day, 50 mg/kg/day was

tolerated. This provided a 10-fold improvement in exposure (total, C_{ave}) over **7f**. For **7n**, bile duct inflammation (at ≥ 50 mg/kg/day), degeneration/regeneration of duodenal or jejunal crypt cell epithelium (at ≥ 150 mg/kg/day) and mortality (at 500 mg/kg/day) were observed in a 14-day toxicity study in rats, and prolongation of PR and QRS intervals in a cardiovascular study in telemetered cynomolgus monkeys (at 75 mg/kg/day) excluded **7n** from further study. Despite the unfavorable hERG profile of **7l**, it emerged as the compound with the best pharmacological profile. Therefore, we sought to understand the in vitro selectivity profile of **7l** versus the previously profiled **7f** and assess its in vivo activity. Of note, using the previously described ribosome binding assay that employs [^{3}H]-**7f** as the radioligand,[18,19] **7l** was found to bind to the 80S isolated ribosomes more weakly than **7f** (Table 4) in spite of comparable activity for the inhibition of PCSK9.

Table 4: Toxicology Summaries for **7f** vs **7l**

Cmpd	Rat Lin(-) IC_{50}/ Human $CD34^+$ IC_{50}	80S K_i (μM)	PCSK9 ELISA IC_{50} (μM)	Hematopoietic cell findings	Total C_{max} (ng/mL)	Total C_{ave} (nM)	NOAEL Total C_{ave} exposure
7f	2.9 μM/2.7 μM	7 μM	0.82	direct 50 mg/kg	1640	2419	478 nM (15 mg/kg)
7l	*65 μM/>20 μM	63 μM	1.37	indirect 150 mg/kg	9660	15869	4231 nM[a] (50 mg/kg)

*puromycin (HPE). [a]free C_{ave} = 1015 nM based on 24% rat plasma protein binding.

In an attempt to understand the difference in overall in vivo toxicity and ribosome binding profiles, ribosome profiling in rat intestinal epithelial cells (IEC-6) was performed. We chose this cell line because of the histopathological intestinal findings with **7f**. IEC-6 cells were found

to have a differential toxicity response to **7l** and **7f** based on a CellTiter-Glo® assay with a high divergence at 4 μM (SI Figure 2). IEC-6 cells were treated with 4 μM **7l** or **7f** for 1 h and direct off-targets were identified using ribosome profiling and our previously described analysis method.[18] In this approach, the cumulative fraction of reads along the annotated protein regions are plotted for the compound treatment and vehicle control. If a compound induced stall occurs, these two plots diverge (SI Figure 2). We define the magnitude of the maximum divergence as D_{max} and the codon at which the maximum divergence occurs as the D_{max} position. If a given protein coding region has a stall, the D_{max} position will be 3' to the stall. For genes with a D_{max} value greater than three standard deviations from the mean, reads 3' to the D_{max} position are extracted and used for differential expression analysis with DESeq. Our previous ribosome profiling study with **7f** demonstrated that the direct effects of compound on translation are observable using ribosome footprint data alone with no changes in transcript levels as measured by mRNA seq[18] so we did not include mRNA-seq in this current study.

Fifty-two IEC-6-expressed nascent chains were found to be sensitive to **7f** with a DESeq false discovery rate of 0.1 and a two-fold decrease in reads mapping 3' to the Dmax position. Eleven **7l**-sensitive nascent chains were detected with the same criteria (Figure 3, SI Table 1). Eight of the **7l**-sensitive nascent chains were also sensitive to **7f** while Ndc80 and Cox15 were only detected for **7l**. All of the off-targets that were identified using one compound were also downregulated by the other compound, albeit not in all cases to the level of a two-fold change and/or an individual false discovery rate of 0.1. With the exceptions of Ndc80 and Cox15, all of the sensitive proteins were more affected by **7f** than **7l** (Figure 3 C-D). Additionally, 49 genes were differentially regulated (false discovery rate < 0.1) upon treatment with **7f** but did not display a buildup of reads indicative of a stall. Most of these displayed an expression level

change in the same direction but with a lower magnitude with **7l** treatment (SI Figure 2). These indirectly-affected proteins likely represent a downstream cellular response. These data indicate that **7f** and **7l** target the same group of direct off-target proteins with **7l** having a much lower effect on all sensitive nascent chains except Ndc80 and Cox15 (Figure 3).

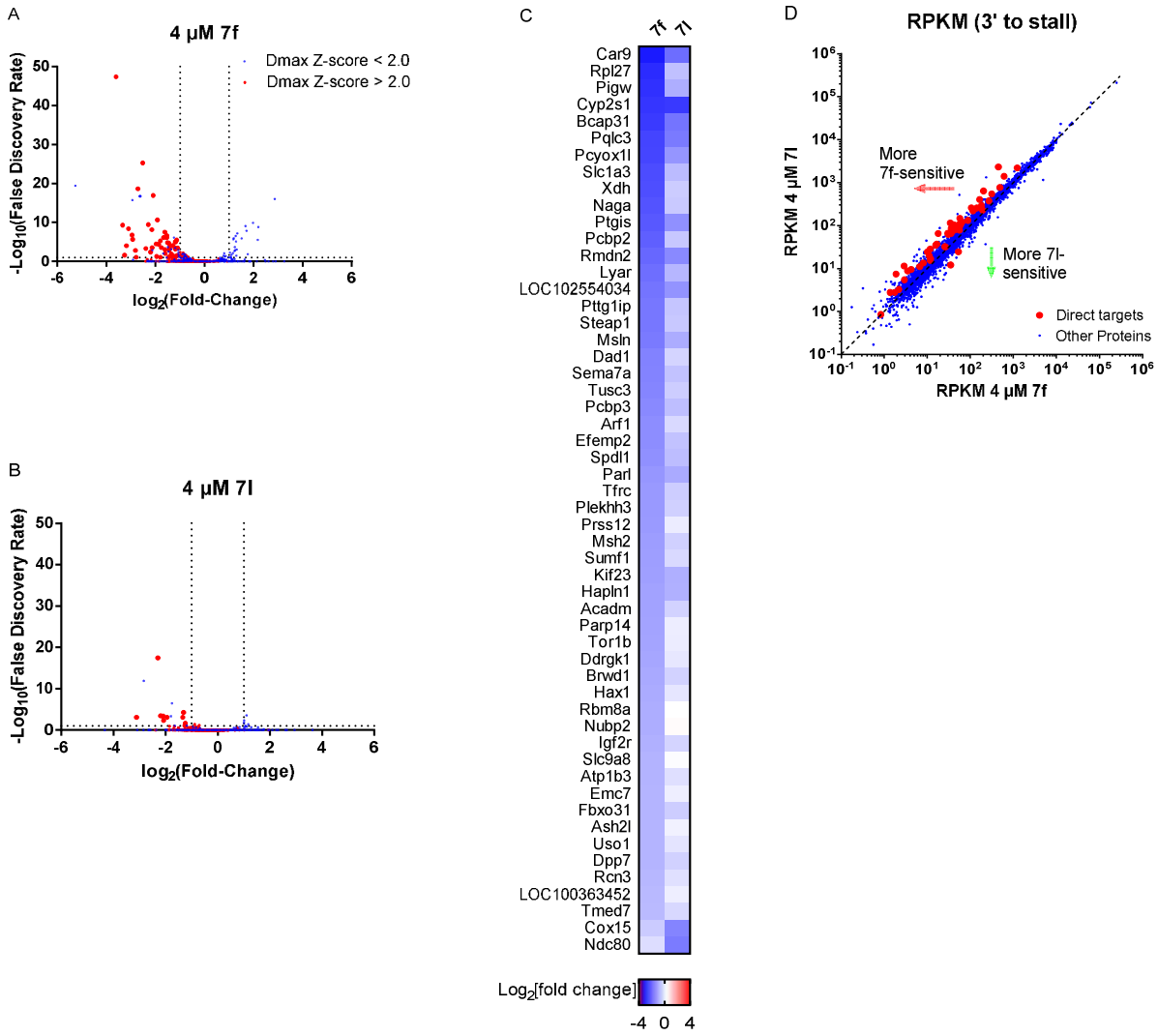

Figure 3. **7l** affects a smaller portion of the translatome than **7f**. Volcano plots of ribosome profiling data from (3A) 4 µM **7f** and (3B) 4 µM **7l**. The points in red indicate genes with a Z-score-transformed Dmax > 2 in either the **7f** or **7l** datasets. Direct off-targets (large red circles) are defined as having a potential buildup of reads to indicate a stall as indicated by a Z-score transformed Dmax > 2, a false discovery rate < 0.1 and at least a two-fold change. (3C) Heatmap displaying the levels of downregulation of compound-sensitive nascent chains. (3D) Scatterplot of protein translation levels in reads per kilobase per million (RPKM) total reads

following treatment with 4 μM **7f** or 4 μM **7l**. The directly affected proteins listed in Figure 3C are represented by a larger red spot. The majority of the directly affected proteins display a lower translation level in the **7f** than the **7l** condition. RPKM values are calculated based on reads aligning 3' to the Dmax position of the Dmax Z-score is greater than 2.0 or 3' to codon 50 otherwise.

The improved rat safety profile for **7l** prompted its assessment of in vivo efficacy in the humanized PCSK9 mouse model. Figure 4 shows relative plasma PCSK9 levels, normalized to t = 0 min, for vehicle, 30 mg/kg and 100 mg/kg doses over 0-24 h. The entire time course was used for determining the concentration-response relationship using an indirect effect PK/PD model. The free C_{eff} for PCSK9 lowering by **7l** was determined to be 175 nM. The ribosome profiling data combined with the improved in vivo safety profile suggested that **7l** was not only more selective, but also a more tolerated variant of **7f**.

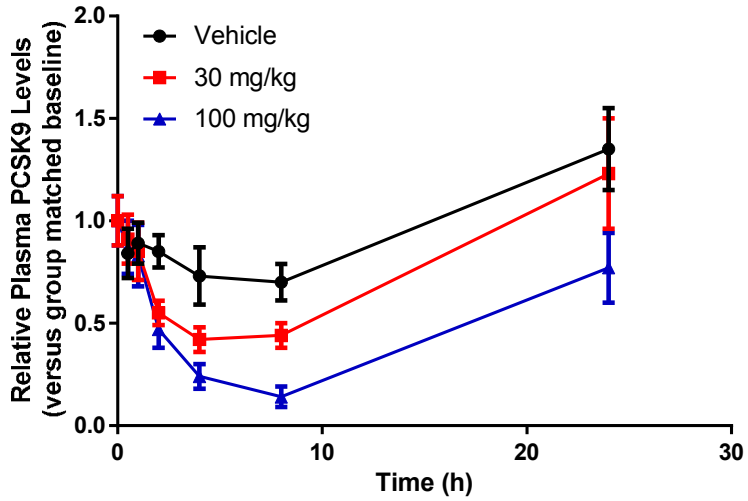

Figure 4: Plasma PCSK9 Levels in hPCSK9 Mice Following Single Oral Dose Administration of **7l**. Data for the 300 mg/kg dose not shown (see SI).

CONCLUSION

We have described an orally active small molecule inhibitor of PCSK9 synthesis designed for systemic exposure that demonstrates an improved in vivo safety profile. Crucial to the expansion of the SAR around progenitor **1** was the development of synthetic methodologies to address the encumbered tertiary amide at the center of the molecule. These chemistries made it possible to efficiently explore alternatives to the isoquinoline and the dihydrocinnamate groups. Library-enabled methods allowed for exploration of each vector. Minimal changes to the head group and amine moiety were tolerated but small changes to the tail fragment resulted in compounds with similar potencies and improved in vivo toxicology profiles. Interestingly, ribosome profiling indicates a change in the degree of stalling of off-target transcripts rather than a significantly altered selectivity profile. While these data are derived from one cell type and it remains unclear whether this pattern is repeated globally to account for the improved overall safety profile. Based on the mode of action for these compounds, a clear challenge for future work will be ensuring sufficient selectivity for inhibition of PCSK9 mRNA translation. A greater understanding of the determinants of translational selectivity will likely be necessary.

EXPERIMENTAL SECTION

All procedures performed on animals in this study were in accordance with established guidelines and regulations, and were reviewed and approved by Pfizer Institutional Animal Care and Use Committee. Pfizer animal care facilities that supported this work are fully accredited by AAALAC International.

Materials and Methods: All chemicals, reagents and solvents were purchased from commercial sources and used without further purification. Compound **2** (CAS # 188111-79-7) was purchased from CNH Technologies (catalog # C-3103R), Woburn, MA. Compound **7f** was

synthesized as previously reported.[18] All reactions were performed under an atmosphere of nitrogen unless otherwise noted. Nuclear magnetic resonance spectra (^{1}H, ^{13}C NMR) were recorded with 400 MHz, 500 MHz or 600 MHz Varian or Bruker spectrometers. Chemical shifts are expressed in parts per million downfield from tetramethylsilane. The peak shapes are denoted as follows: s, singlet; d, doublet; t, triplet; q, quartet; m, multiplet; br s, broad singlet. Due to differences in solvents used in sample preparation and, in some cases amount of water present, not all exchangeable protons were observable. Mass spectrometry (MS) was performed via atmospheric pressure chemical ionization (APCI) or electron scatter (ESI) ionization sources. Silica gel chromatography was performed using a medium pressure Biotage or ISCO system using columns pre-packaged by various commercial vendors including Biotage and ISCO. Whatman pre-coated silica gel plates (250 μm) were used for analytical TLC. Microanalyses were performed by Intertek Pharmaceutical Services and were within 0.4% of the calculated values. All library compounds were > 95% purity as judged by LCMS (UV 254 nm or ELSD detection).

Synthesis

General Procedure A: (Corresponding to Scheme 1, Route A, parallel format). Step 1: To a solution of carboxylic acid (**3**, 125 μmol, 1.0 equiv) in 250 μL DMF was added a solution of 1, 1'-carbonyldiimidazole (250 μL, 0.5 M in DMF). The mixture was shaken at 30 ^{o}C for 1.5 h, then a solution of *tert*-butyl (3*R*)-3-aminopiperidine-1-carboxylate (**2**, 250 μL, 0.5 M in DMF) was added. The reaction was shaken at 30 ^{o}C until complete by LCMS (typically 16 h). The solvents from the crude reaction mixture were evaporated to dryness by Speedvac, the residue was dissolved in DCM (3.0 mL) and washed with water (2 × 3 mL) and brine (3 mL). The organic phase was dried over Na_2SO_4, filtered and concentrated by Speedvac to give the amide

intermediates that were used directly in the next step. Step 2: In a glove box, 2,6-lutidine (32 μL, 276 μmol, 2.2 equiv) was added to a solution of amide (**4**) from Step 1 in 500 μL DCM. The reaction was cooled to -30 ^{o}C, followed by dropwise addition of a solution of trifluoromethanesulfonic anhydride (275 μL, 0.5 M in DCM). The reaction was stirred at -20 ^{o}C for 1.5 h, followed by the addition of a solution of isoquinoline *N*-oxide **5** (200 μL, 0.69M in DCM). The reaction was removed from the glove box. The reaction was shaken at 30 ^{o}C until complete by LCMS (typically 16 h). The solvents from the crude reaction mixture were evaporated by Speedvac and the residue was purified by preparative HPLC to give the *N*-Boc intermediates (**6**). Step 3: A solution of TFA/DCM (2.0 mL, v/v = 1/4) was dispensed into the purified *N*-Boc intermediates from Step 2. After shaking for 1 h at 30 ^{o}C, the solvents were evaporated by Speedvac. The crude material was purified by reversed phase HPLC to afford the desired products (**7**).

General Procedure B: (Corresponding to Scheme 1, Route B, parallel format). Step 1: To the carboxylic acid **3** (0.21 mmol, 1.0 equiv) in DCM (2 mL) was added two drops of DMF followed by oxalyl chloride (21 μL, 0.25 mmol). The reaction was stirred at rt for 2 h and then concentrated. Step 2: The crude acid chloride from Step 1 (~0.21 mmol) was added to a solution of amine **9** (0.11 mmol) in THF (2 mL), *i*Pr_2EtN (96 μL, 0.54 mmol) and DMAP (2 mg). After heating overnight at 65 ^{o}C, the reaction was cooled and poured into saturated $NaHCO_3$, extracted with EtOAc, washed with brine, dried (Na_2SO_4) and concentrated to afford **6**. Step 3: The residue was dissolved in DCM (3 mL) and treated with TFA or HCl (1 mL). After 1 h, the mixture was concentrated. The crude material was either purified by reversed phase HPLC or triturated with diethyl ether (if sufficiently pure after the previous step) to afford the desired

products (**7**).

General Procedure C: (Corresponding to Scheme 1, Route C, parallel format). Step 1: Bromotripyrrolidinophosphonium hexafluorophosphate (PyBroP, 112 mg, 240 μmol, 1.6 equiv), *N*-oxide **11** (150 μmol, 1.0 equiv) and carboxylic acid **3** (180 μmol, 1.2 equiv) were dissolved in 1 mL THF. After addition of *i*Pr_2EtN (70 μL, 450 μmol, 3 equiv), the mixture was shaken at 30 ^oC. After 16 h, the solvent was removed by Speedvac and the residue was submitted to purify by preparative TLC to afford the intermediate (**12**). Step 2: Intermediate **12** (~150 μmol, 1.0 equiv) was dissolved in 1 mL MeOH. Pd-Al_2O_3 (12.5 mg, 10% Pd basis, 12.5 μmol, 0.1 equiv) and triethylsilane (158 μL, 1200 μmol, 8.0 equiv) were then added. The mixture was shaken at 30 ^oC. After 5 h, the reaction mixture was filtered and the filtrate was concentrated by Speedvac to give crude intermediate, which was used in the next step. Step 3: A solution of TFA/DCM (1.0 mL, v/v = 1/4) was dispensed into the crude reaction mixture from Step 2. After shaking for 2 h at 30 ^oC, the solvents were evaporated by Speedvac. The crude material was purified by reversed phase HPLC to afford the desired products (**7**).

General Procedure D: (Corresponding to Scheme 2, parallel format). To a solution of the pinacol boronate **14** (1.0 equiv) in 1,4-dioxane (0.10 M) was added the aryl/heteroaryl halide (100 μmol, 1.0 equiv) followed by Cs_2CO_3 solution (200 μL, 2.0 equiv, 1.0 M) and Pd(dppf)Cl_2 (2 μmol, 0.02 equiv) to each vial under N_2 atmosphere. The reaction was heated under nitrogen at 100 ^oC until complete by LCMS (typically 8-16 h). The solvents from the crude reaction mixture were evaporated by Speedvac. Step 2: A solution of TFA/DCM (2.0 mL, v/v = 1/10) was dispensed into the crude reaction mixture. After shaking for 2 h at 30 ^oC, the solvents were

evaporated by Speedvac. The crude material was purified by reversed phase HPLC to afford the desired products (**7**).

(*R*)-*N*-(isoquinolin-1-yl)-*N*-(piperidin-3-yl)-[1,1'-biphenyl]-4-carboxamide (**7a**). Prepared according to General Procedure A with [1,1'-biphenyl]-4-carboxylic acid. Purified by preparative HPLC (Kromasil Eternity-5-C18 150 × 30 mm × 5 μm; 45-75% acetonitrile: water (0.2% formic acid)) to afford **7a** (13.4 mg, 21%). t_R = 2.80 min, *m/z* = 408 $[M+H]^+$.

(*R*)-*N*-(isoquinolin-1-yl)-*N*-(piperidin-3-yl)-4-(pyrazin-2-yl)benzamide (**7b**). Prepared according to General Procedure B with 4-(pyrazin-2-yl)benzoic acid and *tert*-butyl (*R*)-3-(isoquinolin-1-ylamino)piperidine-1-carboxylate (**9a**). Purified by trituration from diethyl ether to afford **7b** (36 mg, 35%). ^{1}H NMR (400 MHz, MeOH-d_4) δ 8.89 (br s, 1H), 8.56 (br s, 1H), 8.34−8.52 (m, 2H), 7.94−8.19 (m, 2H), 7.57−7.87 (m, 5H), 7.36 (br s, 2H), 4.52−5.05 (m, 1H), 3.45−3.58 (m, 1H), 3.12−3.26 (m, 1H), 2.91 (d, *J* = 10.5 Hz, 2H), 2.26−2.64 (m, 1H), 1.77−1.91 (m, 1H), 1.64 (br s, 2H). LCMS (Method 4) t_R = 0.876 min, *m/z* = 410.0 $[M+H]^+$.

(*R*)-*N*-(isoquinolin-1-yl)-4-(1-methyl-1*H*-pyrazol-4-yl)-*N*-(piperidin-3-yl)benzamide (**7c**). Prepared according to General Procedure D with (*R*)-3-(*N*-(isoquinolin-1-yl)-4-(4,4,5,5-tetramethyl-1,3,2-dioxaborolan-2-yl)benzamido)piperidine-1-carboxylate (**14a**) and 4-bromo-1-methyl-1*H*-pyrazole. Purified by preparative HPLC (Grace Vydac C18 150 × 20 mm × 5 μm; 45-85% acetonitrile: water (0.2% formic acid)) to afford **7c** (7.5 mg, 14%). t_R = 2.34 min; *m/z* = 412 $[M+H]^+$. Analytical HPLC Method 1: t_R = 2.91 min, 99.1%.

(*R*)-*N*-(isoquinolin-1-yl)-*N*-(piperidin-3-yl)-4-(pyrazolo[1,5-*a*]pyrimidin-3-yl)benzamide (**7d**). Prepared according to General Procedure D with **14a** and 3-bromopyrazolo[1,5-*a*]pyrimidine. Purified by preparative HPLC (DIKMA Diamonsil(2) C18 200 × 20 mm × 5 μm; 45-75% acetonitrile: water (0.1% formic acid)) to afford **7d** (9.5 mg, 34%). t_R = 2.45 min; *m/z* = 449 $[M+H]^+$. ^1H NMR (400 MHz, CD_3OD) δ 8.86 (dd, *J* = 1.8, 7.0 Hz, 1H), 8.56 (dd, *J* = 1.8, 4.1 Hz, 1H), 8.48−8.53 (m, 1H), 8.42 (s, 1H), 7.99−8.14 (m, 1H), 7.77−7.91 (m, 4H), 7.68 (br s, 2H), 7.30 (d, *J* = 7.4 Hz, 2H), 7.01 (dd, *J* = 4.1, 7.0 Hz, 1H), 5.27 (br s, 1H), 3.91 (d, *J* = 14.9 Hz, 1H), 3.70−3.81 (m, 1H), 2.88 (br s, 2H), 1.74−2.16 (m, 3H), 1.32 (d, *J* = 17.2 Hz, 1H). Analytical HPLC Method 2: t_R = 3.04 min, 96.8%.

(*R*)-4-(3*H*-[1,2,3]triazolo[4,5-*b*]pyridin-3-yl)-*N*-(isoquinolin-1-yl)-*N*-(piperidin-3-yl)benzamide (**7e**). Prepared according to General Procedure A with 4-(3*H*-[1,2,3]triazolo[4,5-*b*]pyridin-3-yl)benzoic acid. Purified by preparative HPLC (Phenomenex Gemini C18 250 × 21 mm × 10 μm; 45-85% acetonitrile: water (0.2% formic acid)) to afford **7e** (2.5 mg, 4%). t_R = 2.48 min; *m/z* = 450 $[M+H]^+$.

***N*-(3-chloropyridin-2-yl)-*N*-[(3*S*)-piperidin-3-yl]-4-(3*H*-[1,2,3]triazolo[4,5-*b*]pyridin-3-yl)benzamide** (**7g**). Prepared in analogous fashion to **7f** (see SI) with (*S*)-3-[(3-chloropyridin-2-yl)amino]piperidine-1-carboxylate (13.7 g, 86%). [α] = +55.9° (c = 1.965, MeOH). Analytical HPLC Method 3: t_R = 2.47 min, 99.4%.

***N*-(3-chloropyridin-2-yl)-4-(5-methyl-3*H*-[1,2,3]triazolo[4,5-*b*]pyridin-3-yl)-*N*-[(3*R*)-piperidin-3-yl]benzamide** (**7h**). Prepared in analogous fashion to **7f** starting with **9b** and 4-(5-

methyl-3*H*-[1,2,3]triazolo[4,5-*b*]pyridin-3-yl)benzoic acid to afford **7h** hydrochloride. ^{1}H NMR (400 MHz, DMSO-d6) δ 9.34 (br s, 1 H) 8.99 (br s, 1 H) 8.66 (d, *J* = 3.5 Hz, 1 H) 8.55 (d, *J* = 8.6 Hz, 1 H) 8.19 (d, *J* = 8.2 Hz, 1 H) 7.90−8.06 (m, 1 H) 7.44−7.59 (m, 4 H) 5.05 (br s, 1 H) 3.65 (d, *J* = 10.2 Hz, 1 H) 3.15−3.28 (m, 2 H) 2.71 (s, 3 H) 1.71−2.01 (m, 4 H) 1.32 (d, *J* = 8.6 Hz, 1 H). LC (LC-MS Method 1): t_R = 0.59 min. MS (ES+): 448.3 $(M+H)^+$. Elemental Analysis: Calcd for $C_{23}H_{22}ClN_7O \cdot HCl$ C 57.03, H 4.79, N 14.64, Cl 14.64; Found C 56.84, H 4.79, N 19.95, Cl 14.51. Analytical HPLC Method 2: 99.17 %, t_R = 3.33 min.

***N*-(3-chloropyridin-2-yl)-4-(6-methyl-3*H*-[1,2,3]triazolo[4,5-*b*]pyridin-3-yl)-*N*-[(3*R*)-piperidin-3-yl]benzamide** (**7i**). Prepared in analogous fashion to **7f** starting with **9b** (3.2 g, 10.3 mmol) and 4-(6-methyl-3*H*-[1,2,3]triazolo[4,5-*b*]pyridin-3-yl)benzoic acid (2.5 g, 9.8 mmol) to afford **7i** (2.8 g, 90%). ^{1}H NMR ($CDCl_3$) δ 9.53 (br s, 1H), 9.23−8.97 (m, 1H), 8.70 (d, *J* = 1.6 Hz, 1H), 8.67−8.54 (m, 1H), 8.47 (s, 1H), 8.17 (d, *J* = 8.6 Hz, 2H), 8.03−7.88 (m, 1H), 7.53 (d, *J* = 8.6 Hz, 2H), 7.46 (dd, *J* = 4.5, 8.0 Hz, 1H), 5.04 (br s, 1H), 3.63 (d, *J* = 10.9 Hz, 1H), 3.32 (m, 1H), 3.20 (d, *J* = 12.5 Hz, 1H), 2.87−2.63 (m, 1H), 2.50 (s, 3H), 1.96−1.70 (m, 3H), 1.31 (br s, 1H). *m/z* = 449.6 $[M+H]^+$. Elemental Analysis: Calc'd for $C_{23}H_{22}ClN_7O \cdot 1.0\ HCl \cdot 0.1\ H_2O$ C 56.82, H 4.81, N 20.17; Found C 56.69, H 4.61, N 20.15. Analytical HPLC Method 1: t_R = 3.38 min, 99.5 %.

***N*-(3-chloropyridin-2-yl)-*N*-[(3*R*)-piperidin-3-yl]-5-(3*H*-[1,2,3]triazolo[4,5-*b*]pyridin-3-yl)pyridine-2-carboxamide** (**7j**). Prepared in analogous fashion to **7f** starting with **9b** (3.2 g, 10.3 mmol) and 5-(3*H*-[1,2,3]triazolo[4,5-*b*]pyridin-3-yl)pyridine-2-carboxylic acid (2.4 g, 9.8 mmol) to yield **7j** (2.4 g, 98%). ^{1}H NMR (DMSO-d_6) δ 9.23 (br s, 1H), 9.02 (br s, 1H), 8.88 (d,

J = 3.5 Hz, 1H), 8.84−8.63 (m, 2H), 8.56 (d, *J* = 3.1 Hz, 1H), 8.51−8.41 (m, 1H), 8.18 (d, *J* = 9.0 Hz, 1H), 7.94 (d, *J* = 7.4 Hz, 1H), 7.65 (dd, *J* = 8.4, 4.5 Hz, 1H), 7.45 (dd, *J* = 8.0, 4.9 Hz, 1H), 5.14−4.51 (m, 1H), 3.61 (m, 1H), 3.53−3.34 (m, 1H), 3.23 (m, 1H), 2.91−2.64 (m, 1H), 2.23−2.07 (m, 1H), 1.98−1.70 (m, 2H), 1.49−1.34 (m, 1H). *m/z* = 436.9 $[M+H]^+$. Analytical HPLC Method 1: t_R = 2.88 min, 100.0 %.

(*R*)-6-(3*H*-[1,2,3]triazolo[4,5-*b*]pyridin-3-yl)-*N*-(3-chloropyridin-2-yl)-*N*-(piperidin-3-yl)nicotinamide (**7k**). Prepared according to General Procedure C with 6-(3*H*-[1,2,3]triazolo[4,5-*b*]pyridin-3-yl)nicotinic acid and (*R*)-2-((1-(tert-butoxycarbonyl)piperidin-3-yl)amino)-3-chloropyridine 1-oxide (**11**) to afford **7k** (20 mg, 21%). ^{1}H NMR (400 MHz, DMSO-*d6*, 80 ^{o}C) δ 9.20−8.70 (m, 3 H), 8.70 (d, *J* = 8.4 Hz, 1H), 8.68 (d, *J* = 4.0 Hz, 1H), 8.56 (s, 1 H), 8.22 (d, *J* = 8.4 Hz, 1 H), 8.03 (d, *J* = 8.4 Hz, 1 H), 7.96 (d, *J* = 8.4 Hz, 1 H), 7.62 (dd, *J* = 8.0, 4.4 Hz, 1 H), 7.49 (dd, *J* = 8.4, 4.8 Hz, 1 H), 4.90−4.86 (br s, 1 H), 3.65 (m, 1H), 3.29−3.23 (m, 2 H), 2.82−2.77 (m, 1 H), 2.09 (br s, 1H), 1.95−1.80 (br s, 2H), 1.60−1.50 (br s, 1H). LCMS (Method 4) t_R = 0.74 min; *m/z* = 435.2 $[M+H]^+$.

***N*-(3-chloropyridin-2-yl)-5-(6-methyl-3*H*-[1,2,3]triazolo[4,5-*b*]pyridin-3-yl)-*N*-[(3*R*)-piperidin-3-yl]pyridine-2-carboxamide** (**7l**). Prepared in analogous fashion to **7f** starting with **9b** (3.2 g, 10.3 mmol) and 5-(6-methyl-3*H*-[1,2,3]triazolo[4,5-*b*]pyridin-3-yl)pyridine-2-carboxylic acid (2.5 g, 9.8 mmol) to provide **7l** (2.0 g, 98%). ^{1}H NMR (MeOH-d_4, apparent mixture of rotamers) δ 9.27−9.09 (m, 1H), 8.95−8.84 (m, 1H), 8.72 (s, 1H), 8.61−8.50 (m, 1H), 8.49−8.41 (m, 1H), 8.37 (s, 1H), 8.22−8.11 (m, 1H), 8.02−7.80 (m, 1H), 7.54−7.30 (m, 1H), 5.17−4.41 (m, 1H), 3.97−3.60 (m, 2H), 3.56−3.36 (m, 1H), 3.10−2.84 (m, 1H), 2.60 (s, 3H),

2.43−1.80 (m, 3H), 1.74−1.47 (m, 1H). ^{13}C NMR (MeOH-d_4, apparent mixture of rotamers) δ 168.6/167.9, 154.4, 152.1/151.9, 148.6/148.4, 145.1, 141.3, 141.0, 140.1, 139.5, 136.0, 133.2, 131.9, 129.7, 129.3, 127.1, 126.6, 56.1/53.6, 47.6, 45.0, 27.9/26.6, 23.4/23.2, 18.6. *m/z* = 449.4 $[M+H]^+$. Elemental Analysis of the free base: Calc'd for $C_{22}H_{21}ClN_8O \cdot 0.35\ H_2O$ C 58.05, H 4.80, N 24.62, Cl 7.79; Found C 58.22, H 4.57, N 24.38, Cl 7.83. Analytical HPLC Method 1: t_R = 3.19 min, 99.8%.

(*R*)-*N*-(3-chloropyridin-2-yl)-4-(6-(dimethylamino)pyrazin-2-yl)-*N*-(piperidin-3-yl)benzamide (**7m**). To a stirred solution of (*R*)-*tert*-butyl 3-(*N*-(3-chloropyridin-2-yl)-4-(4,4,5,5-tetramethyl-1,3,2-dioxaborolan-2-yl)benzamido)piperidine-1-carboxylate **14b** (1.35 g, 2.5 mmol) in 1,4-dioxane (100 mL) and H_2O (25 mL) was added 6-chloro-*N*,*N*-dimethylpyrazin-2-amine (394 mg, 2.5 mmol) and Na_2CO_3 (800 mg, 7.5 mmol). The reaction mixture was treated with Pd(dppf)Cl_2 (183 mg, 0.25 mmol) under N_2 atmosphere. The mixture was stirred at 100 °C for 3 h. LCMS showed completed reaction. The mixture was concentrated in vacuum and purified by flash chromatography (60% EtOAc: 40% petroleum ether) to afford (*R*)-*tert*-butyl 3-(*N*-(3-chloropyridin-2-yl)-4-(6-(dimethylamino)pyrazin-2-yl)benzamido)piperidine-1-carboxylate (1.2 g, 98.3%), which was then dissolved in DCM (2 mL) and treated with 4N HCl in 1,4-dioxane (10 mL). The mixture was stirred at rt for 30 min and then concentrated in vacuum and triturated with EtOAc to afford **7m** (960 mg, 91.4%) as a yellow solid. ^{1}H NMR (400 MHz, DMSO-*d6*) δ 9.50 (br s, 1H), 9.08 (br s, 1H), 8.62 (br s, 1H), 8.30 (s, 1H), 8.15 (s, 1H), 7.96−7.90 (m, 3H), 7.45 (d, *J* = 4.0, 1H), 7.40 (d, *J* = 4.0 Hz, 1H), 4.90−4.86 (br s, 1H), 3.65 (m, 1H), 3.29 (m, 1H), 3.15 (m, 1H), 3.12 (s, 6H), 2.68 (br s, 1H), 1.89−1.82 (br s, 3H), 1.29 (br s, 1H). *m/z* = 437.1 $[M+H]^+$. Elemental Analysis on the free base: Calc'd for

$C_{23}H_{25}ClN_6O$ C 63.22, H 5.77, N 19.23, Cl 8.11; Found C 63.06, H 5.73, N 19.06, Cl 8.27. Analytical HPLC Method 2: t_R = 2.92 min, 99.5%.

(*R*)-*N*-(3-chloropyridin-2-yl)-4-(6-methylpyrazin-2-yl)-*N*-(piperidin-3-yl)benzamide (**7n**). Prepared in analogous fashion to **7m** starting with **14b** (144 mg, 0.27 mmol) and 2-bromo-6-methylpyrazine (51 mg, 0.29 mmol) to afford **7n** (82 mg, 63%). ^{1}H NMR (MeOH-d_4) δ 8.90 (s, 1H), 8.58 (m, 1H) 8.50 (s, 1H), 7.95 (d, *J* = 7.6 Hz, 2H), 7.77 (d, *J* = 7.6 Hz, 1H), 7.46 (d, *J* = 8.2 Hz, 2H), 7.38 (dd, *J* = 5.0, 7.3 Hz, 1H), 5.07 (t, *J* = 11.7 Hz, 1H), 3.85−3.71 (m, 1H), 3.66 (s, 3H), 3.64−3.56 (m, 1H), 3.36 (d, *J* = 12.9 Hz, 1H), 2.95−2.84 (m, 1H), 2.07−1.97 (m, 1H), 1.90 (m, 1H), 1.52−1.41 (m, 1H), 1.37−1.25 (m, 1H). *m/z* = 408.4 $[M+H]^+$. Elemental Analysis: Calc'd for $C_{22}H_{22}ClN_5O \cdot 2.0\ HCl \cdot 1.7\ H_2O$ C 51.67, H 5.40, N 13.69, Cl 20.80; Found C 51.77, H 5.50, N 13.51, Cl 20.67. Analytical HPLC Method 2: t_R = 2.90 min, 99.1%.

(*R*)-*N*-(3-chloropyridin-2-yl)-4-(6-(methylamino)pyrazin-2-yl)-*N*-(piperidin-3-yl)benzamide (**7o**). Step 1: To a stirred solution of (*R*)-*tert*-butyl 3-(N-(3-chloropyridin-2-yl)-4-(4,4,5,5-tetramethyl-1,3,2-dioxaborolan-2-yl)benzamido)piperidine-1-carboxylate **14b** (0.35 g, 0.65 mmol) in 1,4-dioxane (5 mL) was added 2-bromo-6-chloropyrazine (125 mg, 0.65 mmol) and aq Na_2CO_3 (1.0 mL, 2.0 mmol, 2.0 M). The reaction mixture was treated with Pd(dppf)Cl_2 (52.7 mg, 0.065 mmol), purged with N_2 for 20 min and stirred at 100 °C for 4 h. After cooling to rt, the mixture was diluted with EtOAc, filtered through Celite,® concentrated and purified by flash chromatography (0-100% EtOAc/heptane gradient) to afford (*R*)-*tert*-butyl 3-(*N*-(3-chloropyridin-2-yl)-4-(6-chloropyrazin-2-yl)benzamido)piperidine-1-carboxylate (198 mg, 58 %). Step 2: To a solution the chloropyrazine from Step 1 (32.0 mg, 0.061 mmol) in acetonitrile

(0.51 mL) was added methylamine (0.61 mL, 1.21 mmol, 2.0 M in THF) in a 5 mL microwave vial. The vial was sealed and the reaction was heated to 100 °C. After 64 h, the mixture was cooled to rt and the sample was concentrated under reduced pressure. The crude material was diluted with DCM (1.0 mL) and treated with TFA (82.9 mg, 0.727 mmol, 0.0560 mL). After 16 h, the mixture was concentrated under reduced pressure, diluted with DMSO (1 mL) and purified by reverse-phase chromatography (Atlantis dC18 5μm 4.6 × 50 mm; 50-95% acetonitrile:water (0.05% TFA) to afford 22 mg (57%) of **7o**. t_R = 2.79 min; *m/z* = 423.1 $[M+H]^+$. A larger scale preparation of **7o** was done in analogous fashion to **7m** starting with **14b** and 6-chloro-*N*-methylamino-2-pyrazine. ^{1}H NMR (DMSO-d_6, 600 MHz, apparent mixture of rotamers) δ 9.43 (br s, 1H), 9.05 (br s, 1H), 8.62 and 8.58 (br s, 1H), 8.22 (br s, 1H), 7.91 (d, *J* = 7.6 Hz, 2H), 7.90-7.84 (m, 2H), 7.43 (dd, *J* = 7.6, 4.7 Hz, 1H), 7.32 (d, *J* = 7.6 Hz, 2H), 5.01 (br s, 1H), 3.62-3.55 (m, 1H), 3.47−3.40 (m, 1H), 3.35-3.25 (m, 1H), 3.22−3.15 (m, 1H), 2.85 (s, 3H), 2.77−2.67 (m, 1H), 2.16 (br s, 1H), 1.90−1.84 (m, 1H), 1.34−1.24 (m, 1H). Analytical HPLC Method 3: t_R = 2.33 min, 98.9%.

***tert*-butyl (*R*)-3-(isoquinolin-1-ylamino)piperidine-1-carboxylate (9a)**. To a solution of 1-chloroisoquinoline (5.00 g, 30.6 mmol) and *tert*-butyl (3*R*)-3-aminopiperidine-1-carboxylate (7.34 g, 36.6 mmol) in anhydrous toluene (150 mL) was added *t*-BuOK (10.27 g, 91.7 mmol), (±)-2,2′-bis(diphenylphosphino)-1,1′-binaphthalene (951 mg, 1.53 mmol), and $Pd(OAc)_2$ (343 mg, 1.53 mmol). The reaction mixture was purged with nitrogen three times, and heated at 110 °C overnight. The reaction mixture was cooled to rt and poured into water. The mixture was then extracted with EtOAc (4 x 150 mL). The combined organic layers were dried over anhydrous Na_2SO_4, filtered, and the filtrate was concentrated under reduced pressure. The

resulting dark solid was purified by silica gel column chromatography eluting with a gradient of (10-15%) EtOAc/petroleum ether to deliver **9a** (4.89 g, 49%) as a yellow solid. ^{1}H NMR (400 MHz, $CDCl_3$) δ 7.99 (d, *J* = 5.9 Hz, 1H), 7.74 (d, *J* = 8.4 Hz, 1H), 7.67 (d, *J* = 8.0 Hz, 1H), 7.59 (dd, *J* = 7.5, 7.5 Hz, 1H), 7.45 (dd, *J* = 7.6, 7.6 Hz, 1H), 6.94 (d, *J* = 5.7 Hz, 1H), 5.34 (br s, 1H), 4.33–4.29 (m, 1H), 3.70–3.55 (m, 3H), 3.36–3.30 (m, 1H), 2.04–1.77 (m, 4H), 1.35 (br s, 9H).

***tert*-butyl (3*R*)-3-[(3-chloropyridin-2-yl)amino]piperidine-1-carboxylate** (**9b**). A mixture of 2-bromo-3-chloropyridine (203.8 g, 1.06 moles), sodium *tert*-amylate (147 g, 1.27 moles), *tert*-butyl (3*R*)-3-aminopiperidine-1-carboxylate (249.5 g, 1.25 moles) in toluene (2 L) was heated to 80 °C. To this solution was added chloro(di-2-norbornylphosphino)(2-dimethylaminoferrocen-1-yl) palladium (II) (6.1 g, 10.06 mmol) followed by heating to 105 °C and holding for 3 h. The reaction mixture was cooled to rt, 1 L of water was added, then the biphasic mixture was filtered through Celite®. After layer separation, the organic phase was washed with 1 L of water followed by treatment with 60 g of Darco® G-60 at 50 °C. The mixture was filtered through Celite®, and concentrated to a final total volume 450 mL, resulting in the precipitation of solids. To the slurry of solids was added 1 L of heptane. The solids were collected *via* filtration and then dried to afford **9b** as a dull orange solid (240.9 g, 73%). ^{1}H NMR ($CDCl_3$, 600 MHz) δ 8.03 (d, *J* = 4.7 Hz, 1H), 7.45 (d, *J* = 6.7 Hz, 1H), 6.57−6.51 (m, 1H), 5.08 (br s, 1H), 4.14 (br s, 1H), 3.85−3.30 (m, 4H), 2.00−1.90 (m, 1H), 1.80−1.55 (m, 4H), 1.43 (br s, 9H); ^{13}C NMR ($CDCl_3$, 100.5 MHz) δ 150.0, 153.2, 146.0, 135.9, 115.3, 112.9, 79.5, 48.6, 46.4, 43.7, 29.8, 28.3, 22.4; LCMS (Method 1): t_R = 0.72 min, *m/z* 312.0 $(M+H)^+$; HRMS (*m/z*) $[M+H]^+$ calcd for $C_{15}H_{23}ClN_3O_2$, 312.1473; found, 312.1467.

(*R*)-2-((1-(*tert*-butoxycarbonyl)piperidin-3-yl)amino)-3-chloropyridine 1-oxide (**11**). To a clear solution of 2,3-dichloropyridine (13.0 g, 87.8 mmol) in DCM (130 mL) was added *m*-CPBA (45.5 g, 264 mmol) at 0 ^{o}C. The mixture turned cloudy white. After stirring the mixture at 30 ^{o}C for 32 h, the mixture was concentrated. The crude product was purified by chromatography on silica gel (EtOAc/petroleum ether from 0-80%) to give 2,3-dichloropyridine *N*-oxide (11.1 g, 74%) as a light yellow solid. Step 2: To a light yellow solution of 2,3-dichloropyridine *N*-oxide (4.0 g, 24.4 mmol) in *n*-BuOH (40 mL) was added *tert*-butyl (3*R*)-3-aminopiperidine-1-carboxylate **2** (7.3 g, 36.6 mmol), CsF (3.7 g, 24.4 mmol), *i*Pr$_2$EtN (3.5 g, 27.1 mmol) and DMAP (298 mg, 2.4 mmol) slowly at 0 ^{o}C. The mixture was stirred at 100 °C for 24 h. The mixture was cooled, poured into water (20 mL) and extracted with EtOAc (3 x 150 mL). The combined organic layers were dried over Na_2SO_4, filtered, and concentrated in vacuo. The crude product was purified by silica gel flash column chromatography eluting with a gradient of EtOAc/petroleum ether from (0-60%) to afford **11** (3.9 g, 50%) as a brown oil. ^{1}H NMR (400 MHz, MeOH-d$_4$) δ 8.18 (d, *J* = 6.8 Hz, 1H), 7.53 (d, *J* = 8.1 Hz, 1H), 6.80 (dd, *J* = 6.7,8.3 Hz, 1H), 4.45−4.35 (m, 1H), 3.79−3.70 (m,1H), 3.52−3.38 (m, 3H), 2.08−1.95 (m, 1H), 1.85−1.70 (m, 2H), 1.60−1.50 (m, 1H), 1.47 & 1.40 (s, 9H, *rotamers*). LCMS (Method 3): t_R = 1.18 min, *m/z* = 327.9 $[M+H]^+$.

***tert*-butyl (*R*)-3-(4-bromo-*N*-(isoquinolin-1-yl)benzamido)piperidine-1-carboxylate** (**13a**). To a suspension of 4-bromobenzoic acid (3.30 g, 16.4 mmol) in anhydrous DCM (120 mL) was added oxalyl chloride (6.26 g, 49.3 mmol) dropwise at 0 °C followed by 3 drops of DMF. The resulting mixture was stirred at rt for 2 h. The mixture was then concentrated in vacuo to give 4-bromobenzoyl chloride as a yellow solid. The solid was dissolved in anhydrous THF (40 mL)

and a solution of **9a** (4.89 g, 14.9 mmol) in anhydrous THF (50 mL) was added. The resulting solution was treated with LHMDS (44.8 mL, 44.8 mmol, 1 M) dropwise at 0 °C. The reaction mixture was stirred at rt overnight. The mixture was poured into water and extracted with EtOAc (4 x 100 mL). The combined organic layers were dried over Na_2SO_4, filtered, and the filtrate was concentrated under reduced pressure. The crude product was purified by silica gel chromatography eluting with a gradient of (0-25%) EtOAc/petroleum ether to afford **13a** (4.80 g, 63%) as a yellow solid. ^{1}H NMR (400 MHz, $CDCl_3$, mixture of rotamers) δ 8.42 (s, 1H), 7.98–7.83 (m, 1H), 7.73 (d, 1H), 7.65–7.47 (m, 3H), 7.10–7.06 (m, 4H), 4.94–4.45 (m, 2H), 4.26–3.91 (m, 1.5H), 3.50–3.45 (m, 0.5H), 2.65–2.15 (m, 2H), 1.86–1.56 (m, 3H), 1.52 & 1.43 (s, 9 H).

***tert*-butyl (3*R*)-3-[(4-bromobenzoyl)(3-chloropyridin-2-yl)amino]piperidine-1-carboxylate** (**13b**). Compound **9b** (214.4 g, 687.7 mmol) was dissolved in 260 mL of THF and the resulting suspension was cooled to -10 ^{o}C. LHMDS (1 M in THF, 687.7 mL, 687.1 mmol) was added over 25 min followed by warming to 20 ^{o}C and stirring for 1 h before cooling back to -10 ^{o}C. 4-Bromobenzoyl chloride (140.0 g, 625.2 mmol) was added as a solution in 230 mL of THF over 1.5 h, maintaining the internal temperature at less than -7 ^{o}C. After complete addition, the reaction mixture was warmed to 0 ^{o}C at which point HPLC indicated the reaction was complete. MeOH was added (101 mL), then the reaction was warmed to rt and concentrated in vacuo to a low volume. The solvent was then exchanged to 2-MeTHF. The crude product solution was washed with 700 mL of half-saturated aq $NaHCO_3$, followed by 200 mL of half-saturated brine. The 2-MeTHF solution was concentrated to a low volume followed by addition of 400 mL of heptane resulting in precipitation of solids which were collected *via* filtration. The collected solids were dried to afford **13b** as a tan powder (244 g, 79% yield). ^{1}H NMR (CD_3CN) δ

8.57−8.41 (m, 1H), 7.85−7.62 (m, 1H), 7.34 (d, *J* = 5.9 Hz, 2H), 7.28 (dd, *J* = 7.6, 4.7 Hz,1H), 7.24−7.16 (m, 2H), 4.63−4.17 (m, 2H), 4.06−3.89 (m, 1H), 3.35−3.08 (br s, 0.5H), 2.67−2.46 (m, 1H), 2.26−2.10 (br s, 0.5H), 1.92−1.51 (m, 3H), 1.46 (s, 9H), 1.37−1.21 (m, 1H).

***tert*-butyl (*R*)-3-(*N*-(isoquinolin-1-yl)-4-(4,4,5,5-tetramethyl-1,3,2-dioxaborolan-2-yl)benzamido)piperidine-1-carboxylate (14a).** To a suspension of **13a** (3.7 g, 7.2 mmol), bis(pinacolato)diboron (3.68 g, 14.5 mmol) and KOAc (2.14 g, 21.8 mmol) in 1,4-dioxane (25 mL) was added $PdCl_2$(dppf) (0.53 g, 0.73 mmol). The resulting mixture was purged with N_2 and heated at 80-90 °C for 4 h. The reaction was cooled and concentrated under reduced pressure. The crude compound was purified by silica gel flash chromatography eluting with a gradient of petroleum ether: EtOAc (50: 1 to 1.5:1) to give a yellow gum. The yellow gum was triturated with petroleum ether and filtered to afford **14** (3.8 g, 94%) as a white solid. ^{1}H NMR (400 MHz, MeOH-d_4, mixture of rotamers) δ 8.46 (br s, 0.75H), 8.38 (br s, 0.25H), 8.08 (br s, 0.25H), 7.99 (br s, 0.75H), 7.83 (br s, 1H), 7.79–7.61 (m, 4H), 7.33 (br s, 2H), 7.21 (br s, 2H), 4.65–4.58 (m, 1H), 4.28–4.25 (m, 1H), 4.04–3.96 (m, 1H), 3.45–3.40 (m, 1H), 2.67–2.55 (m, 1H), 2.30–2.09 (m, 1H), 1.87−1.84 (m, 1H),1.51 (s, 5.4H), 1.42 (s, 3.6H), 1.26 (s, 7.2H), 1.22 (s, 4.8H).

***tert*-butyl (3*R*)-3-{(3-chloropyridin-2-yl)[4-(4,4,5,5-tetramethyl-1,3,2-dioxaborolan-2-yl)benzoyl]amino}piperidine-1-carboxylate (14b).** To a solution of **13b** (40.0 g, 80.8 mmol) in 1,4-dioxane (250 mL) were added bis(pinacolato)diboron (41.1 g, 162 mmol), KOAc (23.8 g, 244 mmol) and $PdCl_2$(dppf) (5.9 g, 8.1 mmol). The resulting mixture was purged with N_2 and stirred at 80-90 ^{o}C for 10 h. The reaction was cooled and filtered. The organic solution was concentrated in vacuo. The residue was purified by silica gel column chromatography, eluting with a gradient of 2-25% EtOAc/petroleum ether to give the title compound as a yellow gum.

The yellow gum was triturated with petroleum ether to afford **14b** as a white solid (30 g, 69%). ^{1}H NMR (MeOH-d_4) δ 8.52 (br s, 1H), 7.74 (br s, 1H), 7.55 (br s, 2H), 7.31 (br s, 3H), 4.53 (br s, 1H), 4.30 (br s, 1H), 4.05–4.02 (br m, 1H), 2.80–2.29 (br m, 2H), 1.95–1.68 (m, 3H), 1.50 (br s, 10 H), 1.32 (br s, 12H). LCMS (Method 1): t_R = 1.12 min, *m/z* 542.1 $(M+H)^+$.

4-(3*H*-[1,2,3]triazolo[4,5-*b*]pyridin-3-yl)benzoic acid (**20a**). Step 1: To a solution of 2-chloro-3-nitropyridine (95.0 g, 0.600 mol) and ethyl 4-aminobenzoate (99.0 g, 0.600 mol) in toluene (3 L) was added K_2CO_3 (166 g, 1.20 mol), (±)-2,2′-bis(diphenylphosphino)-1,1′-binaphthalene (7.40 g, 11.8 mmol), $Pd(OAc)_2$ (2.80 g, 12.5 mmol) and NaI (2.70 g, 18.0 mmol). The mixture was stirred at 110 ^{o}C, for 6 h. The reaction mixture was cooled to 30 ^{o}C, filtered through Celite®, and the filtrate was concentrated in vacuo. The residue was transferred to a separatory funnel with water (300 mL) and extracted with EtOAc (3 x 300 mL). The organic layers were dried over Na_2SO_4, filtered and the filtrate was concentrated in vacuo to give a dark solid residue, which was washed with acetone/water (5/1, 100 mL) and filtered to afford a yellow solid (142 g, 82%).^{1}H NMR (DMSO-d_6) δ 8.60−8.57 (m, 2H), 7.95 (d, *J* = 8.0 Hz, 2H), 7.88 (d, *J* = 8.0 Hz, 2H), 7.12 (dd, *J* = 4.7, 2.1 Hz, 1H), 4.31 (q, *J* = 8.0 Hz, 2H), 1.33 (t, *J* = 8.0 Hz, 3H). Step 2: To a solution of ethyl 4-((3-nitropyridin-2-yl)amino)benzoate from Step 1 (120 g, 0.417 mol), in ethanol (2.00 L), was added Raney-Ni (30 g). The reaction mixture was hydrogenated under a H_2 atmosphere (50 psi) at 30 ^{o}C for 20 h. The mixture was filtered through Celite®. The filtrate was dried over Na_2SO_4, filtered, and the filtrate was concentrated in vacuo to afford a yellow solid. The yellow solid was washed with DCM to give a yellow solid (75 g, 70%). ^{1}H NMR (DMSO-d_6) δ 10.05 (br, 1H), 7.94 (d, *J* = 8.0 Hz, 2H) 7.54 (d, *J* = 4.0 Hz, 1H), 7.46 (d, *J* = 8.0 Hz, 2H), 7.40 (d, *J* = 8.0 Hz, 1H), 7.15−7.05 (m, 1H), 4.30 (q, *J* = 8.0 Hz, 2H), 1.31 (t, *J* = 8.0 Hz, 3H). Step 3: To a solution of ethyl 4-((3-aminopyridin-2-yl)amino)benzoate from Step 2 (70.0 g,

0.272 mol) in a mixture of AcOH (70 mL) and water (70 mL), was added $NaNO_2$ (23.8 g, 0.345 mol) at 0 °C. The mixture was stirred at 30 °C for 20 min. The mixture was diluted with DCM (100 mL), washed with water (3 x 50 mL). The organic phase was dried over Na_2SO_4, filtered, and the filtrate was concentrated in vacuo to afford a dark solid. The solid was washed with acetone (30 mL) to afford a white solid (63 g, 86%). ^{1}H NMR (DMSO-d_6) δ 9.14 (d, *J* = 4.0 Hz, 1H), 8.91 (d, *J* = 4.0 Hz, 1H), 8.50 (d, *J* = 8.0 Hz, 2H), 8.24 (d, *J* = 8.0 Hz, 2H), 7.66 (dd, *J* = 8.5, 4.2 Hz, 1H), 4.37 (q, *J* = 8.0 Hz, 2H), 1.36 (t, *J* = 8.0 Hz, 3H). Step 4: To a solution of ethyl 4-(3*H*-[1,2,3]triazolo[4,5-*b*]pyridin-3-yl)benzoate from Step 3 (60.0 g, 0.224 mol) in MeOH (700 mL), was added 2N NaOH (260 mL, 0.520 mmol). The mixture was stirred at 60 °C for 2 h. The mixture was acidified with 1N HCl to pH ~ 1. The reaction mixture was extracted with EtOAc (3 x 100 mL). The combined organic layers were dried over Na_2SO_4, filtered, and the filtrate was concentrated in vacuo to afford the title compound as a white solid (52 g, 97%). ^{1}H NMR (DMSO-d_6, 600 MHz) *δ* 13.23 (br s, 1H), 8.91 (d, *J* = 4.0 Hz, 1H), 8.76 (d, *J* = 8.0 Hz, 1H), 8.48 (d, *J* = 8.0 Hz, 2H), 8.24 (d, *J* = 8.0 Hz, 2H), 7.68−7.65 (m, 1H); ^{13}C NMR (DMSO-d_6, 100.5 MHz) *δ* 166.5, 151.6, 144.7, 139.2, 137.4, 130.9, 130.1, 129.4, 121.1, 120.5; HRMS (*m/z*) $[M+H]^+$ calcd for $C_{12}H_9N_4O_2$, 241.0720; found, 241.0719.

4-(5-methyl-3*H*-[1,2,3]triazolo[4,5-*b*]pyridin-3-yl)benzoic acid (**20b**). Prepared in analogous fashion to 4-(3*H*-[1,2,3]triazolo[4,5-*b*]pyridin-3-yl)benzoic acid with 2-chloro-6-methyl-3-nitropyridine to afford the title compound as a brown solid. ^{1}H NMR (DMSO-d_6) δ 8.57 (d, *J* = 8.8 Hz, 1H), 8.34 (d, *J* = 8.8 Hz, 2H), 8.20 (d, *J* = 8.8 Hz, 2H), 7.50 (d, *J* = 8.2 Hz, 1H), 2.73 (s, 3H).

4-(6-methyl-3*H*-[1,2,3]triazolo[4,5-*b*]pyridin-3-yl)benzoic acid (**20c**). Prepared in analogous fashion to 4-(3*H*-[1,2,3]triazolo[4,5-*b*]pyridin-3-yl)benzoic acid with 2-chloro-5-methyl-3-

nitropyridine (10.0 g, 57.9 mmol) to afford the title compound as a brown solid (10.5 g, 90%). ^{1}H NMR (DMSO-d_6) δ 8.78 (s, 1H), 8.54 (s, 1H), 8.48 (d, *J* = 4.4 Hz, 2H), 8.24 (d, *J* = 4.4 Hz , 2H), 2.56 (s, 3H).

5-(3*H*-[1,2,3]triazolo[4,5-*b*]pyridin-3-yl)pyridine-2-carboxylic acid (**20d**). Step 1: To a solution of 5-aminopicolinic acid (13.5 g, 97.7 mmol) in anhydrous ethanol (200 mL) was added $SOCl_2$ (60.0 mL, 504 mmol) dropwise at 0 ^oC under N_2 atmosphere. The resulting mixture was heated at reflux and stirred overnight. The reaction mixture was concentrated in vacuo. The residue was dissolved in a saturated aqueous $NaHCO_3$ solution so that that pH of the solution was approximately pH 9-10. The reaction mixture was extracted with EtOAc (8 x 250 mL). The combined organic phases were dried over Na_2SO_4, filtered, and concentrated in vacuo to afford a brown solid (14.3 g, 88%). ^{1}H NMR ($CDCl_3$) δ 8.14 (s, 1H), 7.94 (d, J = 8.4 Hz, 1H), 6.97 (d, J = 8.0 Hz, 1H), 4.41 (q, J = 7.2 Hz, 2H), 4.16 (br s, 2H), 1.39 (t, J = 7.2 Hz, 3H). Steps 2-4: Prepared in analogous fashion to 4-(3*H*-[1,2,3]triazolo[4,5-*b*]pyridin-3-yl)benzoic acid with 2-chloro-3-nitropyridine (15.2 g, 95.9 mmol) to afford the title compound as a red solid (8.1 g, 99%). ^{1}H NMR ($CDCl_3$) δ 13.50 (br s, 1H), 9.62 (d, 1H), 8.93−8.87 (m, 2H), 8.77 (d, *J* = 8.4 Hz 1H), 8.36 (d, J = 8.4 Hz ,1H), 7.68 (dd, *J* = 8.7, 4.7 Hz, 1H).

6-(3*H*-[1,2,3]triazolo[4,5-*b*]pyridin-3-yl)nicotinic acid (**20e**). Prepared in analogous fashion to 4-(3*H*-[1,2,3]triazolo[4,5-*b*]pyridin-3-yl)benzoic acid with ethyl 6-aminonicotinate (3.25 g, 30.0 mmol) to afford the title compound as a brown solid (430 mg, 78%). ^{1}H NMR (DMSO-d_6) δ 13.8 (br s, 1H), 9.27 (s, 1H) 9.00 (d, *J* = 4.0 Hz, 1H), 8.85 (d, *J* = 8.0 Hz, 1H), 8.73 (m, 1H), 8.58 (d, *J* = 8.0 Hz, 1H), 7,76 (dd, *J* = 4.0, 8.0 Hz, 1H).

5-(6-methyl-3*H*-[1,2,3]triazolo[4,5-*b*]pyridin-3-yl)pyridine-2-carboxylic acid (**20f**). Prepared in analogous fashion to 4-(3*H*-[1,2,3]triazolo[4,5-*b*]pyridin-3-yl)benzoic acid starting from ethyl

5-aminopicolinate (14.0 g, 84.2 mmol) and 2-chloro-5-methyl-3-nitropyridine (17.4 g, 101 mmol) to afford the title compound as a red solid (10.8 g 95%). ^{1}H NMR (DMSO-d_6) δ 13.50 (br s, 1H), 9.63 (d, *J* = 2.3 Hz, 1H), 8.89 (dd, *J* = 8.6, 2.3 Hz, 1H), 8.81 (d, *J* = 1.6 Hz, 1H), 8.55 (s, 1H), 8.37 (d, *J* = 8.6 Hz, 1H), 2.55 (s, 3H).

Luciferase Reporter Assay. The human PCSK9 prodomain (amino acids 1-152) was fused to firefly luciferase cDNA (amino acids 2-550) in pcDNA3.1 and stably transfected into human hepatocarcinoma (Huh7) cells. Huh7 ProLuc cells were maintained in Dulbecco's Modified Eagle's medium (DMEM) with 4.5 g/L glucose supplemented with 10% fetal bovine serum (FBS), L-glutamine, penicillin/streptomycin and 900 μg/mL Geneticin. On the day of the assay, cells were plated at 10,000 cells per well in 384 well plates (Greiner 781080) in DMEM phenol red free media with 10% FBS, L-glutamine and penicillin/streptomycin. Cells were incubated for 4 h at 37 °C in 5% CO_2. 5 μL of test compound diluted in media was added to the cell plate (final compound top dose concentration in assay is 20 μM in 0.5 % DMSO). In addition to these test compound conditions each screening plate included wells that contained 20 μM of compound **1** as a positive assay control defined as high percent effect (HPE), as well as wells containing media in 0.5% DMSO as a negative treatment control defined as zero percent effect (ZPE). Cells were incubated overnight at 37 °C in 5% CO_2. Plates were removed from the incubator and equilibrated for 30 min at rt before adding 25 μL of SteadyGlo reagent. After 30 min the plates were read on an EnVision plate reader (Perkin Elmer) using the enhanced luminescence setting. Values were normalized utilizing the ZPE and HPE output and IC_{50} was calculated and reported as the midpoint in the percent effect curve in molar units.

ELISA for secreted PCSK9. Huh7 cells were maintained at 70-80% confluence in the growing media consisting of high-glucose DMEM, 10% FBS (BSA-free, Sigma-Aldrich), 2 mM L-glutamine and 1% penicillin-streptomycin (Life Technologies) at 37 °C, 5% CO_2. A custom AlphaLISA (Perkin Elmer) assay was developed for PCSK9. For PCSK9, two Pfizer proprietary monoclonal antibodies targeting PCSK9 recognizing different epitopes within mature PCSK9 were utilized, one biotinylated and one conjugated to the Alphabead. Huh7 cells were plated at 7,500 cells/well in 384-well cell culture plates containing 2 μL vehicle, or test compounds. The final assay volume was 20 μL. Cells were incubated overnight (16-20 h) at 37 °C in a 5% CO_2 atmosphere and the levels of PCSK9 in cell culture media were determined by direct addition of detection reagents. 5 μL of the respective biotinylated antibody (3 nM final concentration) and antibody-conjugated Alphabeads (10 μg/mL final concentration) in assay buffer were added to the cell plate. After a 0.5 h incubation at rt, 5 μL of streptavidin donor beads (40 μg/mL final) were added to the cell plate and incubation continued for an additional 1 h at rt. Plates were then read on an EnVision plate reader using Alphascreen settings with Ex = 680 nm, Em = 615 nm.

Rat Bone Marrow Lineage (-) cell toxicity assay

Rat bone marrow was collected by flushing isolated rat femurs and tibia with PBS/2% FBS/2 mM EDTA. Cells were dissociated into single cell populations and lysed with red blood cell lysis buffer. The remaining cells were washed and then blocked with anti-CD16/CD32 and human Fc blocks. Biotinylated antibodies to rat CD3, rat CD11b, rat CD45R and erythroid were added to capture differentiated cells and then streptavidin capture beads were added. The cell suspension was run through a MidiMACS LS magnetic column (Miltenyi Biotec) and the rat hematopoietic progenitor (rat lineage (-)) bone marrow cells were collected in the run through.

Cells were plated at 7,500 cells per 18 μL in assay media (Iscove's Modified Dulbecco's Medium supplemented with 20% fetal bovine serum, penicillin/streptomycin, 2 mM glutamine, CC 100 Cytokine Cocktail and rat granulocyte-macrophage colony-stimulating factor) into the 384 well Culturplate and incubated for 24 hours at 37° C in 5% CO_2 prior to compound treatment. The serially diluted compounds were added to a Costar 384 well plate as 2 μL per well to make a near assay ready plate. In addition to these test compounds, each screening plate included wells that contained 10 mM (20 μM final). Puromycin or **7f** were as a positive assay control HPE, and wells containing DMSO (0.5% final) as a negative treatment control defined as ZPE. The near assay ready plate containing 2 μL of the compound was diluted with 38 μL of assay media and 2 μL from the interim compound plate was transferred into the Culturplate assay plates containing cells. The final assay volume was 20 μL with 20000, 10000, 5000, 2500, 1250, 625, 312, 156, 78, 39, 19 nM compound in 0.5% DMSO. The plate was spun at 300 rpm for 1 min and the cells were then incubated for 72 h with compound at 37° C in 5% CO_2. At the end of the 72 h incubation the cell plates were removed from the incubator and placed at rt for 20-30 min to equilibrate. CellTiter Glo® was added as 20 μL per well to the plates and incubated for 30 min. The plates were read on an EnVision plate reader using the enhanced luminescence setting.

$CD34^+$ Cell Viability Assay

An ex-vivo human hematopoietic progenitor cell $CD34^+$ cytotoxicity assay was utilized to identify compounds with reduced toxicity and improved selectivity. Cells were plated at 7,500 cells per 18 μL in assay media containing cytokine differentiation mix into a 384 well Viewplate and incubated for 24 h at 37° C in 5% CO_2 prior to compound treatment. Test compounds were serially diluted in an eleven point, 0.5 log dilution format in DMSO before further dilution into media. 2 μL from the compound plate were added to the cell plate. Test compounds at a final

concentration of 100 μM were incubated with cells for 72 h. In addition, each screening plate also included wells that contained 100 μM **7f** as a positive assay control defined as HPE, as well as wells containing media in 0.5% DMSO as a negative treatment control defined as ZPE. Viability was determined using the CellTiter Glo® ATP detection system following manufacturer's instructions. Values obtained were then normalized incorporating the ZPE and HPE results and IC_{50} reported as the midpoint in the percent effect curve in molarity.

ASSOCIATED CONTENT

Supporting Information

HPLC and LC-MS conditions, description of in vitro and ex vivo assay systems, PCSK9 assay statistics, ribosome profiling protocols and data, python scripts, hPCSK9 mouse exposure data, and molecular formula strings. This material is available free of charge via the Internet at http://pubs.acs.org.

AUTHOR INFORMATION

Corresponding Authors

*Phone: (860) 715-6150, E-mail: allyn.londregan@pfizer.com, Phone: (860) 686-0271, E-mail: david.w.piotrowski@pfizer.com.

Author Contributions

The manuscript was written through contributions of all authors. All authors have given approval to the final version of the manuscript.

Funding Sources

The authors declare the following competing financial interest(s): Pfizer Medicinal Chemistry. The funder played a role in study design, data collection and analysis, decision to publish, and preparation of the manuscript. Pfizer Emerging Science Fund. The funder played a role in study design, data collection and analysis, decision to publish, and preparation of the manuscript. National Institutes of Health (grant number S10-RR029668). Funding supported experiments by NGL. The funder had no role in study design, data collection and analysis, decision to publish, or preparation of the manuscript. National Institutes of Health (grant number S10-RR027303). Funding supported experiments by NGL. The funder had no role in study design, data collection and analysis, decision to publish, or preparation of the manuscript. National Institutes of Health (grant number P50-GM102706). Received by NGL and JHDC.

Notes

The authors declare the following competing financial interest(s): This work was funded in-part by Pfizer. ATL, LW, JX, DP, RGD, KFM, MWB, JSW, SBC, CL, JG, BAT, KDH, GEA, BR, CTS, JRC, SL and DWP were employed by Pfizer Inc at the time this work was done. Data availability: Sequencing data and processed files from the ribosome profiling experiments are available through the NCBI gene expression omnibus (Accession GSE110426).

ACKNOWLEDGMENT

This work used the Vincent J. Coats Genomics Sequencing laboratory at the University of California, Berkeley, supported by National Institutes of Health (NIH) S10 Instrumentation Grants S10RR029668 and S10RR027303, as well as computing resources of the Center for RNA Systems Biology (NIH grant P50-GM102706). The authors thank Neal Sach, Mark Barrila,

Sophie Lavergne, Edward L. Conn, Etzer Darout, Sandra Jennings, Thomas A. Brandt, Christopher S. Jones and Jeffrey W. Raggon for their chemistry contributions, David Lloyd, Carol Petras, Natalia Schmidt and Kristen Ford for their contributions to construction of the ProLuc cell line and screening of compounds in the assay, Kevin Beaumont, Karen Atkinson and Dennis Scott for PK, and Amanda King-Ahmad for bioanalysis of in vivo samples. Paula Loria is acknowledged for her helpful suggestions.

ABBREVIATIONS

EGF-A, epidermal growth factor precursor homology domain A; HLM, human liver microsomes; HPE, high percent effect; LDLR, low density lipoprotein receptor; MDCK Madin-Darby canine kidney; PCSK9, proprotein convertase subtilisin/kexin type 9; RLM, rat liver microsomes; RRCK, Ralph Russ canine kidney; siRNA, short interfering RNA; TPSA, topological polar surface area; ZPE, zero percent effect.

REFERENCES

[1] Park, S. W.; Moon, Y. A.; Horton, J. D. Post-transcriptional regulation of low density lipoprotein receptor protein by proprotein convertase subtilisin/kexin type 9a in mouse liver. *J. Biol. Chem.* **2004**, *279*, 50630−50638.

[2] (a) Cunningham, D.; Danley, D. E.; Geoghegan, K. F.; Griffor, M. C.; Hawkins, J. L.; Subashi, T. A.; Varghese, A. H.; Ammirati, M. J.; Culp, J. S.; Hoth, L. R.; Mansour, M. N.; McGrath, K. M.; Seddon, A. P.; Shenolikar, S.; Stutzman-Engwall, K. J.; Warren, L. C.; Xia, D.; Qiu, X. Structural and biophysical studies of PCSK9 and its mutants linked to familial hypercholesterolemia. *Nat. Struct. Mol. Biol.* **2007**, *14*, 413−419. (b) Piper, D. E.; Jackson, S.;

Liu, Q.; Romanow, W. G.; Shetterly, S.; Thibault, S. T.; Shan, B.; Walker, N. P., The crystal structure of PCSK9: a regulator of plasma LDL-cholesterol. *Structure* **2007**, *15*, 545−552. (c) Surdo, P. L.; Bottomley, M. J.; Calzetta, A.; Settembre, E. C.; Cirillo, A.; Pandit, S.; Ni, Y. G.; Hubbard, B.; Sitlani, A.; Carfi, A. Mechanistic implications for LDL receptor degradation from the PCSK9/LDLR structure at neutral pH. *EMBO Rep.* **2011**, *12*, 1300−1305.

[3] Zhang, D. W.; Lagace, T. A.; Garuti, R.; Zhao, Z.; McDonald, M.; Horton, J. D.; Cohen, J. C.; Hobbs, H. H. Binding of proprotein convertase subtilisin/kexin type 9 to epidermal growth factor-like repeat A of low density lipoprotein receptor decreases receptor recycling and increases degradation. *J. Biol. Chem.* **2007**, *282*, 18602−18612.

[4] DeVay, R. M.; Shelton, D. L.; Liang, H. Characterization of proprotein convertase subtilisin/kexin type 9 (PCSK9) trafficking reveals a novel lysosomal targeting mechanism via amyloid precursor-like protein 2 (APLP2). *J. Biol. Chem.* **2013**, *288*, 10805−10818.

[5] Cohen, J. C.; Boerwinkle, E.; Mosley, T. H.; Hobbs, H. H. Sequence variations in PCSK9, low LDL, and protection against coronary heart disease. *N. Engl. J. Med.* **2006**, *354*, 1264−1272.

[6] Giugliano, R. P.; Sabatine, M. S. Are PCSK9 inhibitors the next breakthrough in the cardiovascular field? *J. Am. Coll. Cardiol.* **2015**, *65*, 2638−2651.

[7] Seidah, N. G.; Prat, A. The biology and therapeutic targeting of the proprotein convertases. *Nat. Rev. Drug Discov.* **2012**, *11*, 367−383.

[8] Pingali, H.; Kalapatapu, V. V. M. S.; Makadia, P.; Jain, M. R. Compounds for the Treatment of Dyslipidemia and Related Diseases. PCT Int. Appl. WO 2011051961, 2011.

[9] Du, F.; Hui, Y.; Zhang, M.; Linton, M. F.; Fazio, S.; Fan, D. Novel domain interaction regulates secretion of proprotein convertase subtilisin/kexin type 9 (PCSK9) protein. *J. Biol. Chem.* **2011**, *286*, 43054−43061.

[10] (a) McNutt, M. C.; Lagace, T. A.; Horton, J. D. Catalytic activity is not required for secreted PCSK9 to reduce low density lipoprotein receptors in HepG2 cells. *J. Biol. Chem.* **2007**, *282*, 20799−20803. (b) Li, J.; Tumanut, C.; Gavigan, J. A.; Huang, W. J.; Hampton, E. N.; Tumanut, R.; Suen, K. F.; Trauger, J. W.; Spraggon, G.; Lesley, S. A.; Liau, G.; Yowe, D.; Harris, J. L. Secreted PCSK9 promotes LDL receptor degradation independently of proteolytic activity. *Biochem. J.* **2007**, *406*, 203−207.

[11] (a) Holla, O. L.; Cameron, J.; Tveten, K.; Strom, T. B.; Berge, K. E.; Laerdahl, J. K.; Leren, T. P. Role of the C-terminal domain of PCSK9 in degradation of the LDL receptors. *J. Lipid Res.* **2011**, *52*, 1787−1794. (b) Yamamoto, T.; Lu, C.; Ryan, R. O. A two-step binding model of PCSK9 interaction with the low density lipoprotein receptor. *J. Biol. Chem.* **2011**, *286*, 5464−5470.

[12] (a) Schroeder, C. I.; Swedberg, J. E.; Withka, J. M.; Rosengren, K. J.; Akcan, M.; Clayton, D. J.; Daly, N. L.; Cheneval, O.; Borzilleri, K. A.; Griffor, M.; Stock, I.; Colless, B.; Walsh, P.; Sunderland, P.; Reyes, A.; Dullea, R.; Ammirati, M.; Liu, S.; McClure, K. F.; Tu, M.; Bhattacharya, S. K.; Liras, S.; Price, D. A.; Craik, D. J. Design and synthesis of truncated EGF-A peptides that restore LDL-R recycling in the presence of PCSK9 in vitro. *Chem. Biol. (Oxford, U. K.)* **2014**, *21*, 284−294. (b) Zhang, Y.; Eigenbrot, C.; Zhou, L.; Shia, S.; Li, W.; Quan, C.; Tom, J.; Moran, P.; Di Lello, P.; Skelton, N. J.; Kong-Beltran, M.; Peterson, A.; Kirchhofer, D. Identification of a small peptide that inhibits PCSK9 protein binding to the low density

lipoprotein receptor. *J. Biol. Chem.* **2014**, *289*, 942−955. (c) Taechalertpaisarn, J.; Zhao, B.; Liang, X.; Burgess, K. Small molecule inhibitors of the PCSK9·LDLR interaction. *J. Am. Chem. Soc.* **2018**, *140*, 3242−3249.

[13] Zhang, Y.; Ultsch, M.; Skelton, N. J.; Burdick, D. J.: Beresini, M. H.; Li, W.; Kong-Beltran, M.; Peterson, A.; Quinn, J.; Chiu, C.; Wu, Y.; Shia, S.; Moran, P.; Di Lello, P.; Eigenbrot, C.; Kirchhofer, D. Discovery of a cryptic peptide-binding site on PCSK9 and design of antagonists. *Nat. Struct. Mol. Biol.* **2017**, *24*, 848–856.

[14] Pettersen, D.; Fjellström, O. Small molecule modulators of PCSK9 – A literature and patent overview. *Bioorganic Med. Chem. Lett*. **2018**, *28*, 1155−1160.

[15] Chorba, J. S.; Shokat, K. M. The proprotein convertase subtilisin/kexin type 9 (PCSK9) active site and cleavage sequence differentially regulate protein secretion from proteolysis. *J. Biol. Chem.* **2014**, *289*, 29030−29043.

[16] (a) van Poelgeest, E. P.; Swart, R. M.; Betjes, M. G.; Moerland, M.; Weening, J. J.; Tessier, Y.; Hodges, M. R.; Levin, A. A.; Burggraaf, J. Acute kidney injury during therapy with an antisense oligonucleotide directed against PCSK9. *Am. J. Kidney Dis.* **2013**, *62*, 796−800. (b) Fitzgerald, K.; Frank-Kamenetsky, M.; Shulga-Morskaya, S.; Liebow, A.; Bettencourt, B. R.; Sutherland, J. E.; Hutabarat, R. M.; Clausen, V. A.; Karsten, V.; Cehelsky, J.; Nochur, S. V.; Kotelianski, V.; Horton, J.; Mant, T.; Chiesa, J.; Ritter, J.; Munisamy, M.; Vaishnaw, A. K.; Gollob, J. A.; Simon, A. Effect of an RNA interference drug on the synthesis of proprotein convertase subtilisin/kexin type 9 (PCSK9) and the concentration of serum LDL cholesterol in

healthy volunteers: a randomised, single-blind, placebo-controlled, phase 1 trial. *Lancet* **2014**, *383*, 60−68.

[17] Petersen, D. N.; Hawkins, J.; Ruangsiriluk, W.; Stevens, K. A.; Maguire, B. A.; O'Connell, T. N.; Rocke, B. N.; Boehm, M.; Ruggeri, R. B.; Rolph, T.; Hepworth, D.; Loria, P. M.; Carpino, P. A. A small-molecule anti-secretagogue of PCSK9 targets the 80S ribosome to inhibit PCSK9 protein translation. *Cell Chem. Biol*., **2016**, *23*, 1362–1371.

[18] Lintner, N. G.; McClure, K. F.; Petersen, D.; Londregan, A. T.; Piotrowski, D. W.; Wei, L.; Xiao, J. ; Bolt, M.; Loria, P. M.; Maguire, B.; Geoghegan, K. F.; Huang, A.; Rolph, T.; Liras, S.; Doudna, J. A.; Dullea, R. G.; Cate, J. H. D. Selective stalling of human translation through small-molecule engagement of the ribosome nascent chain. *PLoS Biol.* **2017**, *15*, e2001882/1−e2001882/36.

[19] McClure, K. F.; Piotrowski, D. W.; Petersen, D.; Wei, L.; Xiao, J.; Londregan, A. T.; Kamlet, A.; Dechert-Schmitt, A.-M.; Raymer, B.; Ruggeri, R. B.; Canterbury, D.; Limberakis, C.; Liras, S.; DaSilva-Jardine, P.; Dullea, R. G.; Loria, P. M.; Reidich, B.; Salatto, C. T.; Eng, H.; Kimoto, E.; Atkinson, K.; King-Ahmad, A.; Scott, D.; Beaumont, K.; Chabot, J. R.; Bolt, M.; Maresca, K.; Dahl, K.; Arakawa, R.; Takano, A.; Halldin, C. Liver-targeted small molecule inhibitors of proprotein convertase subtilisin/kexin type 9 synthesis. *Angew. Chem. Int. Ed.* **2017**, *56*, 16218–16222.

[20] Di, L. W.-P., C.; Umland, J. P.; Zhang, H.; Zhang, X.; Gebhard, D. F.; Lai, Y.; Federico, J. J.; Davidson, R. E.; Smith, R.; Reyner, E. L.; Lee, C.; Feng, B.; Rotter, C.; Varma, M. V.;

Kempshall, S.; Fenner, K.; El-Kattan, A. F.; Liston, T. E.; Troutman, M. D. Development of a new permeability assay using low-efflux MDCKII cells. *J. Pharm. Sci.* **2011**, *100*, 4974−4985.

[21] (a) Abramovitch, R. A.; Singer, G. M. Direct alkyl and aryl amination of heteroaromatic nitrogen compounds. *J. Am. Chem. Soc.* **1969**, *91*, 5672−5673. (b) Abramovitch, R. A.; Singer, G. M. Direct acylamination of pyridine 1-oxides. *J. Org. Chem.* **1974**, *39*, 1795−1802. (c) Abramovitch, R. A.; Rogers, R. B. Direct acylamination of 3-substituted pyridine-1-oxides. Directive effect of the substituent. *J. Org. Chem.* **1974**, *39*, 1802−1807. (d) Abramovitch, R. A.; Pilski, J.; Konitz, A.; Tomasik, P. Direct acylamination of pyridine 1-oxide with N-phenylarenimidoyl chlorides and fluorides. *J. Org. Chem.* **1983**, *48*, 4391−4393. (e) Manley, P. J.; Bilodeau, M. T. A mild method for the formation and in situ reaction of imidoyl chlorides: conversion of pyridine-1-oxides to 2-aminopyridine amides. *Org. Lett.* **2002**, *4*, 3127−3129. (f) Couturier, M.; Caron, L.; Tumidajski, S.; Jones, K.; White, T. D. Mild and direct conversion of quinoline N-oxides to 2-amidoquinolines with primary amides. *Org. Lett.* **2006**, *8*, 1929−1932.

[22] (a) Londregan, A. T.; Piotrowski, D. W.; Xiao, J. Rapid and selective in situ reduction of pyridine-N-oxides with tetra-hydroxydiboron. *Synlett* **2013**, *24*, 2695−2700. (b) Balicki, R. $TiCl_4$/NaI - a novel, efficient reagent for mild reduction of the N−O bond in amine N-oxides and nitrones. *Chem. Ber.* **1990**, *123*, 647−648.

[23] Londregan, A. T.; Storer, G.; Wooten, C.; Yang, X.; Warmus, J. An improved amide coupling procedure for the synthesis of N-(pyridin-2-yl)amides. *Tetrahedron Lett.* **2009**, *50*, 1986−1988.

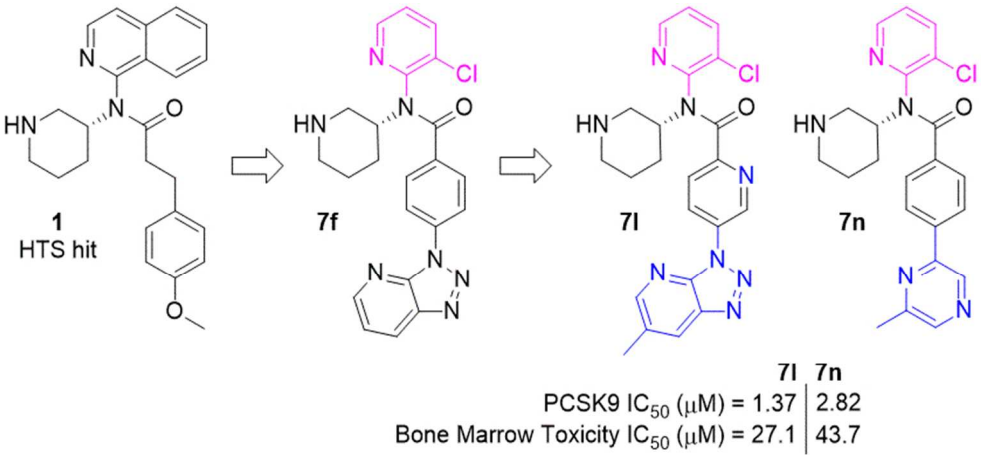

Table of Contents Graphic

226x101mm (96 x 96 DPI)